6 Spin-Orbital Entanglement in Mott Insulators

Andrzej M. Oleś
Institute of Theoretical Physics
Jagiellonian University
Prof. Stanisława Łojasiewicza 11, Kraków, Poland

Contents

E. Pavarini and E. Koch (eds.)
Orbital Physics in Correlated Matter
Modeling and Simulation Vol. 13
Forschungszentrum Jülich, 2023, ISBN 978-3-95806-689-2
http://www.cond-mat.de/events/correl23

1 Entangled superexchange: SU(2) ⊗ SU(2) model

1.1 Spin-orbital Hilbert space in a Mott insulator

At large on-site Coulomb repulsion U, electrons in a transition metal oxide localize and have no kinetic energy. The new state of electronic matter which emerges under strong Coulomb repulsion is a Mott insulator. Then the electron state is given by the spin component and the orbital occupied by this electron. It was one of the great achievements of Kugel and Khomskii [1] to realize that in the case of two orbitals available at each site i, the Hilbert space of a Mott insulator is spanned by spin-orbital states, i.e., it suffices to specify a spin and a pseudospin (orbital) component of each electron to define its quantum state at site i. Such localized electrons in the absence of kinetic energy interact by superexchange [2, 3].

To illustrate these concepts, we begin with a study of a one-dimensional (1D) spin-orbital superexchange model $\mathcal{H}_{\rm SE}$ defined in a Mott insulator with on-site repulsion U by the spin-orbital Hilbert space spanned by the eigenstates $\{|\uparrow\rangle, |\downarrow\rangle\}$, of spin $S = 1/2$, and orbital (pseudospin) operator $T = 1/2$, with the eigenstates $\{|+\rangle, |-\rangle\}$. Such states at two neighboring sites i and $i+1$ are coupled by 1D spin-orbital ('Kugel-Khomskii') superexchange [4–6],

$$\mathcal{H}_{\rm SE} = J \sum_i \left[\left(\mathbf{S}_i \cdot \mathbf{S}_{i+1} + \alpha \right) \left(\mathbf{T}_i \cdot \mathbf{T}_{i+1} + \beta \right) - \alpha\beta + \varepsilon_z \sum_i \tau_i^{(c)} \right], \tag{1}$$

where $\tau_i^{(c)} = T_i^{(c)} = \sigma_i^z/2$, and we take the orbital splitting $J\varepsilon_z = E_z = 0$. Here a constant term $\alpha\beta$ is eliminated and the Hamiltonian $\mathcal{H}_{\rm SE}$ includes only operator terms. The 1D kinetic energy is given by the orbital-flavor (α=+, −) conserving hopping $\propto t$, and the interaction energy is given by either $U n_{i\alpha\uparrow} n_{i\alpha\downarrow}$ or $U n_{i\alpha\sigma} n_{i\alpha\bar{\sigma}}$, which both cost the Coulomb repulsion energy U. Of particular interest is the strongly correlated regime $U \gg t$, where electrons localize and interact by antiferromagnetic (AF) superexchange [2],

$$J = \frac{4t^2}{U}. \tag{2}$$

For two degenerate orbitals one needs to introduce a doubly-degenerate Hubbard model [7]. One finds then again the same exchange constant J (2) as in the derivation of the t-J model from the Hubbard model in the limit $U \gg t$ [8].

It was a great achievement to realize that spin and orbital states are entangled and are parts of the same Hilbert space [9, 10]. Thus the superexchange $\mathcal{H}_{\rm SE}$ in Eq. (1) is not just a scalar product of two involved subspaces, spin and orbital, but describes joint quantum fluctuations of these two operators [9–12]. The superexchange model (1) depends on two parameters $\{\alpha, \beta\}$, and they decide about the type of order. It describes a competition between four spin-orbital phases, where the order in each sector can be either ferro- or antiferro-. The phases where quantum fluctuations exist in the ground state only in at most one sector (spin or orbital) are disentangled, as the phases I-III, see the phase diagram in Fig. 1. Otherwise, we recognize one entangled phase IV-VI which has three different regimes. Here spin-orbital entanglement increases when the quantum critical point (QCP) $(-1/4, -1/4)$ is approached along the diagonal

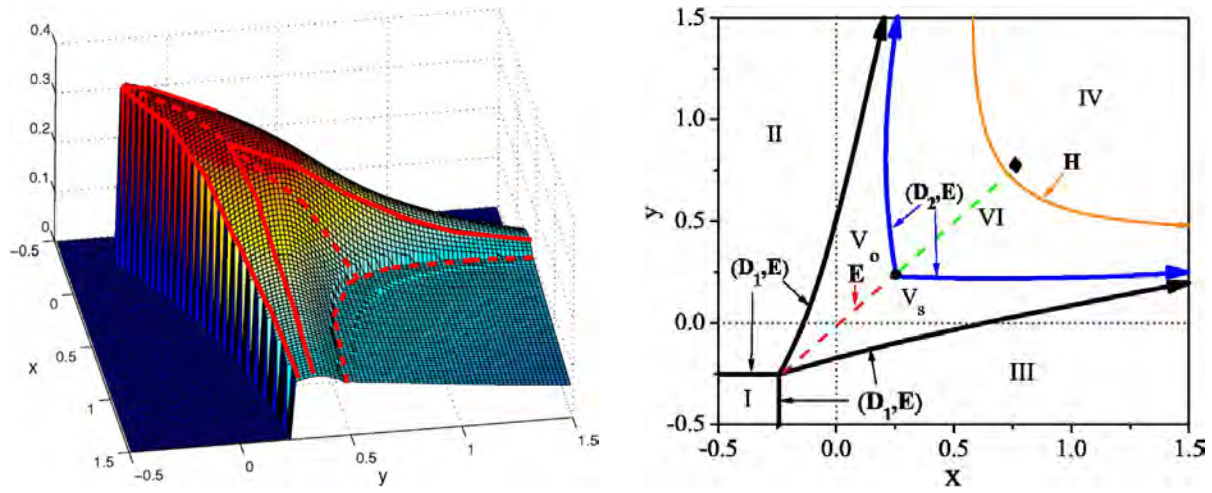

Fig. 1: *Spin-orbital entanglement in the 1D SU(2) ⊗ SU(2) model (1) at $E_z = 0$. Left—The von Neumann entropy per site $\mathcal{S}_{vN}/L$ (3) for the ground state at $L = 8$ as a function of x and y. The phase boundaries (solid and dashed lines) are drawn to guide the eye. Right—Phase diagram of a coupled 1D spin-orbital chain. The diamond point is located at $(3/4, 3/4)$. Quantum phases are distinguished by entanglement: I, II, and III are disentangled, IV is weakly, and V& VI stronger entangled. The parameters (x, y) are the same as (α, β) in Fig. 2. Images after Ref. [6].*

line $x = y$. At the QCP itself, spin-orbital entanglement is maximal within the phase V, changes to a plateau in IV, and next drops towards zero in IV beyond the QCP ($\alpha = \beta < -1/4$).

A standard measure of entanglement between two subsystems A and B in the ground state $|\mathrm{GS}\rangle$ of a system of size L is the von Neumann entropy [13]: $\mathcal{S}_{\mathrm{vN}} = -\mathrm{Tr}_A\{\rho_A \ln \rho_A\}/L$, see Fig. 1. Here our two subsystems are spins and orbitals and the entanglement concerns the entire system (in other applications the system would frequently be separated into A and B by cutting one bond). The von Neumann entropy is obtained by integrating the density matrix, $\rho_A = \mathrm{Tr}_B|\mathrm{GS}\rangle\langle\mathrm{GS}|$ over subsystem B. Consequently, we use here the following definition of the von Neumann spin-orbital entanglement entropy:

$$\mathcal{S}_{\mathrm{vN}} = -\frac{1}{L}\mathrm{Tr}_S\{\rho_S \ln \rho_S\}, \tag{3}$$

where

$$\rho_S = \mathrm{Tr}_T|\mathrm{GS}\rangle\langle\mathrm{GS}| \tag{4}$$

is the reduced spin-only density matrix (4), with the orbital $\{T\}$ degrees of freedom being integrated out.

1.2 Modifications due to finite spin-orbit coupling λ

Spin and orbital operators may also couple directly on-site via the spin-orbit interaction [14]. It is in general quantum but we present the Ising coupling here for more clarity. Then the 1D model Hamiltonian consists of two qualitatively distinct terms [15],

$$\mathcal{H} = \mathcal{H}_{\mathrm{SE}} + \mathcal{H}_{\mathrm{SOC}}, \tag{5}$$

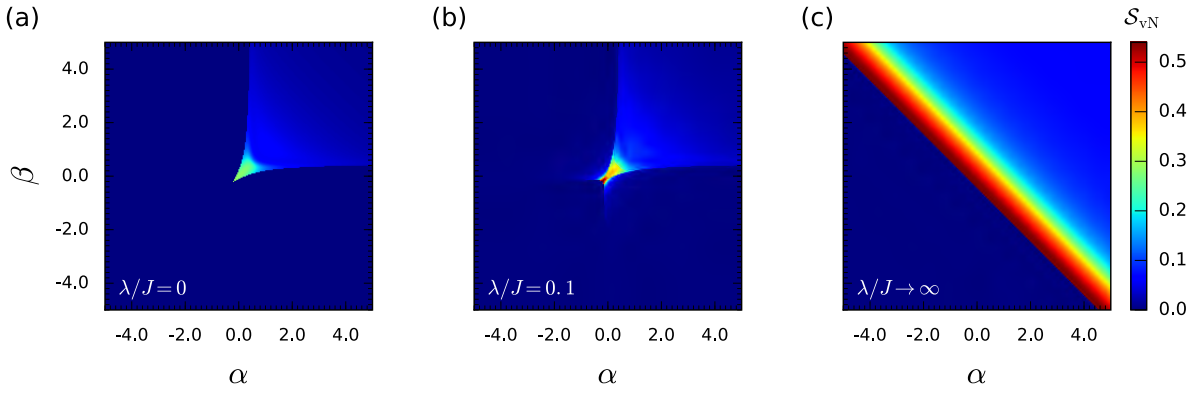

Fig. 2: *The von Neumann spin-orbital entanglement entropy, $\mathcal{S}_{\rm vN}$ (3), calculated using ED on an L=12-site periodic chain for the spin-orbital model Eq. (5) and for the increasing value of the spin-orbit coupling λ [15]: (a) $\lambda/J=0$, (b) $\lambda/J=0.1$, and (c) $\lambda/J\to\infty$.*
Image by courtesy of Dorota Gotfryd.

and includes next to the superexchange $\mathcal{H}_{\rm SE}$ (1), the spin-orbit Ising interaction $\propto\lambda$. The model Hamiltonian (5) depends then on three parameters $\{\alpha,\beta,\lambda\}$. Altogether, our choice means that the spin-orbital exchange interaction has the simplest possible form that can, nevertheless, simulate a realistic situation found in the transition metal oxides. We note that the spin-orbital exchange (1) would have in general a more complex form. For instance, this would be the case if, e.g. three instead of two active orbitals were taken into account, and the corrections from finite Hund's exchange were included (as relevant for the $5d$ iridates).
The second term in Eq. (5) stands for the on-site spin-orbit coupling (SOC) and reads,

$$\mathcal{H}_{\rm SOC}=2\lambda\sum_i S_i^z T_i^z. \tag{6}$$

Here the parameter λ measures the strength of the on-site spin-orbit coupling (of relativistic origin). The above Ising form of the spin-orbit coupling was chosen as the simplest possible and yet nontrivial term. Moreover, exactly such a form of the spin-orbit coupling is *typically* realized in systems with *two* active orbitals. This is the case, for instance, of the active t_{2g} doublets in YVO_3 [16, 17] and Sr_2VO_4 [18], or in optical lattices [19]. In fact, such a highly anisotropic form of spin-orbit coupling is valid for any system with an active orbital doublet, either two directional p (p_x and p_y) or two planar t_{2g} (xz and yz) orbitals.
The line $\beta{=}{-}\alpha$ plays a special role in the phase diagram of Fig. 1. In order to better understand the physical consequences of increasing λ, we display the onset of the spin-orbital entanglement once $\beta{=}{-}\alpha$. As shown in Fig. 2 for increasing λ, the region of finite spin-orbital entanglement increases dramatically and includes both previously disentangled phases, II and III [15]. In fact, the largest entanglement is found in the vicinity of the line $\beta{=}{-}\alpha$, when $\alpha{+}\beta>-1/4$. At $\alpha{+}\beta=-1/4$ the spin-orbital entanglement entropy jumps from $\mathcal{S}_{\rm vN}=0$ to a maximal value and that happens at the QCP. Thus, the qualitative result of Fig. 1 breaks down. We conclude that finite spin-orbit coupling transfers on-site entanglement to on-bond entanglement in the phases antiferromagnetic/ferro-orbital (AF/FO, phase II) and ferromagnetic/alternating-orbital (FM/AO, phase III) which are initially disentangled (at $\lambda{=}0$, see Fig. 3.)

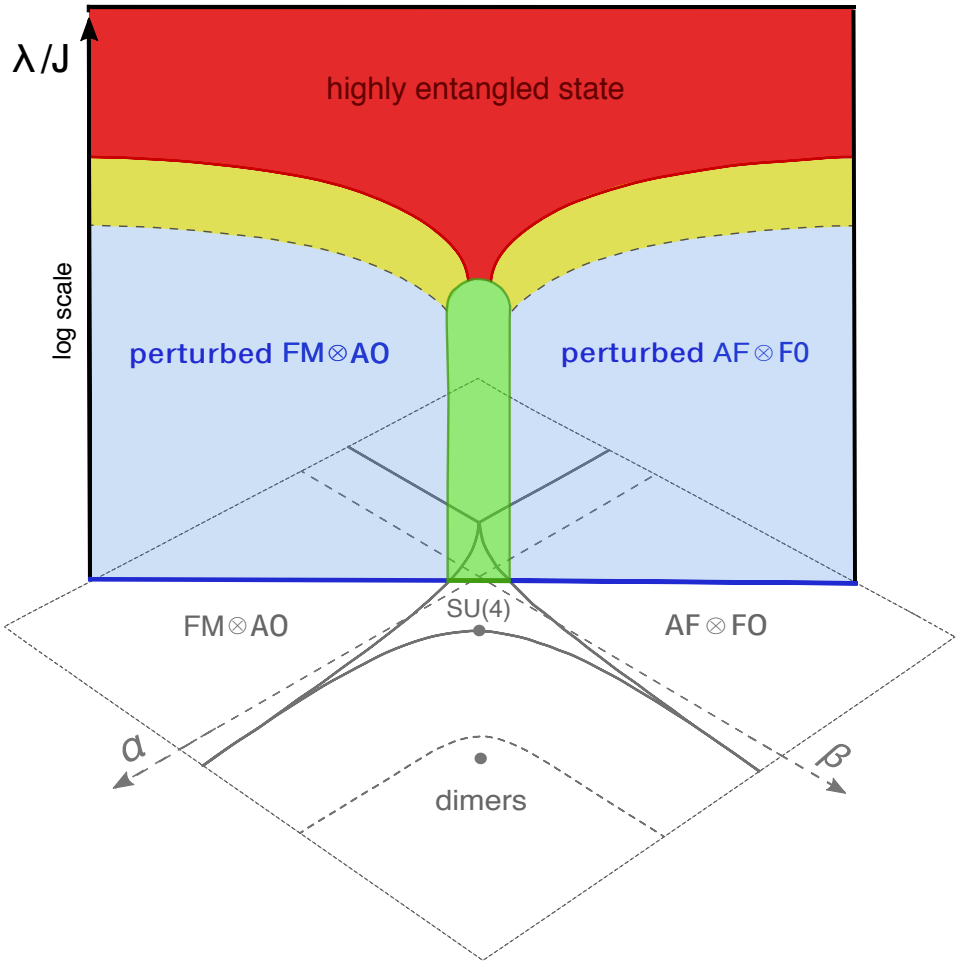

Fig. 3: *Schematic quantum phase diagram of Hamiltonian (1) in the* (α, β) *plane, see Fig. 1. The colorful vertical plane shows how spin-orbital entanglement extends to the highly entangled state, with on-bond entanglement in two disentangled phases: FM⊗AO and AF⊗FO, see Fig. 2. Increasing spin-orbit coupling* λ *generates on-bond entangled states (the green region marks entangled states; note that the vertical scale is logarithmic). Image reproduced from Ref. [15].*

2 Orbital physics for partly filled e_g orbitals

It is important to realize that modeling of transition-metal oxides [3] can be performed on different levels of sophistication. We shall present here some effective orbital-only and spin-orbital superexchange models for correlated $3d$ orbitals. In a perovskite lattice they are coupled by hopping t between nearest neighbor ions, while the hopping to more distant neighbors and for other lattices may be generated using the general rules formulated by Slater and Koster [20]. The orbitals have particular shapes and belong to two irreducible representations of the O_h cubic point group:
(i) a two-dimensional (2D) representation of e_g-orbitals $\{|3z^2{-}r^2\rangle/\sqrt{6},\ |x^2{-}y^2\rangle/\sqrt{2}\}$, and
(ii) a three-dimensional (3D) representation of t_{2g}-orbitals $\{|xy\rangle, |yz\rangle, |zx\rangle\}$.
In the absence of any tetragonal distortion or crystal-field (CF) due to surrounding oxygens, the $3d$-orbitals are degenerate within each irreducible representation of the O_h point group and

have typically a large splitting $\propto 10D_q \approx 2.0$ eV between them. When some of such degenerate orbitals are partly filled, electrons (or holes) have both spin and orbital degree of freedom. The kinetic energy H_t in a perovskite follows from the hybridization between $3d$- and $2p$-orbitals. In an effective d-orbital model, the oxygen $2p$-orbitals are not included explicitly and we define the largest hopping element t obtained between two orbitals of the same type, which both belong to the nearest neighbor $3d$ ions in a lattice.

We begin with conceptually simpler t_{2g} orbitals where finite hopping t results from the d-p hybridization along π-bonds and each element couples a pair of identical orbitals active along a given bond. Each t_{2g} orbital is active along two cubic axes, while the hopping is forbidden along the axis perpendicular to the plane of this orbital, e.g. the hopping between two xy-orbitals vanishes along the c axis (due to the cancellations caused by orbital phases). It is therefore convenient to introduce the following short-hand notation for the orbital degree of freedom [12],

$$|a\rangle \equiv |yz\rangle, \qquad |b\rangle \equiv |zx\rangle, \qquad |c\rangle \equiv |xy\rangle. \tag{7}$$

The labels $\gamma = a, b, c$ refer here to the cubic axes where the hopping is absent between two orbitals of a given type,

$$H_t(t_{2g}) = -t \sum_{\alpha} \sum_{\langle ij\rangle \| \gamma \neq \alpha} a^{\dagger}_{i\alpha\sigma} a_{j\alpha\sigma}, \tag{8}$$

Here $a^{\dagger}_{i\alpha\sigma}$ is an electron creation operator in a t_{2g}-orbital $\alpha \in \{yz, zx, xy\}$ with spin $\sigma = \uparrow, \downarrow$ at site i, and the local electron density operator for a spin-orbital state is $n_{i\alpha\sigma} = a^{\dagger}_{i\alpha\sigma} a_{i\alpha\sigma}$. For t_{2g} electrons not only spin but also orbital flavor is conserved in each hopping process $\propto t$.

The hopping Hamiltonian for e_g electrons concerns σ-bands and couples here two directional e_g-orbitals $\{|i\zeta_\gamma\rangle, |i\zeta_\gamma\rangle\}$ along a bond $\langle ij\rangle \parallel \gamma$ (we use again the same notation t) [21],

$$H_t(e_g) = -t \sum_{\alpha} \sum_{\langle ij\rangle \| \alpha, \sigma} a^{\dagger}_{i\zeta_\alpha\sigma} a_{j\zeta_\alpha\sigma}. \tag{9}$$

Indeed, a hopping with amplitude $-t$ between two sites i and j occurs only when an electron with spin σ transfers between the two directional orbitals $|\zeta_\gamma\rangle$ oriented along the bond $\langle ij\rangle$ direction, i.e., $|\zeta_\gamma\rangle \propto |3x^2{-}r^2\rangle$, $|3y^2{-}r^2\rangle$, or $|3z^2{-}r^2\rangle$, along the cubic axis $\gamma = \{a, b, c\}$. We will similarly denote by $|\xi_\gamma\rangle$ an orthogonal orbital to $|\zeta_\gamma\rangle$. It is perpendicular to the bond $\langle ij\rangle$ direction, i.e., $|\xi_\gamma\rangle \propto |y^2{-}z^2\rangle$, $|z^2{-}x^2\rangle$, and $|x^2{-}y^2\rangle$ along the cubic axis $\gamma \in \{a, b, c\}$, and $\langle \xi_\gamma | \zeta_\gamma \rangle = 0$. For the moment we consider only electrons with one spin component, $\sigma = \uparrow$, to focus on the orbital problem. While such a choice of an over-complete basis $\{\zeta_a, \zeta_b, \zeta_c\}$ is convenient, for writing down the kinetic energy a particular orthogonal basis is needed.

The usual choice is to take

$$|z\rangle \equiv \tfrac{1}{\sqrt{6}}|3z^2{-}r^2\rangle, \qquad |\bar{z}\rangle \equiv \tfrac{1}{\sqrt{2}}|x^2{-}y^2\rangle, \tag{10}$$

i.e., the basis of *real* e_g *orbitals* [21]. However, this basis is the natural one only for the bonds parallel to the c-axis but not for those within the (a, b) plane, and for $\uparrow$-spin electrons the hopping reads (here for clarity we omit spin index σ),

$$H^{\uparrow}_t(e_g) = -\frac{1}{4}t \sum_{\langle mn\rangle \| ab} \left[3a^{\dagger}_{i\bar{z}} a_{j\bar{z}} + a^{\dagger}_{iz} a_{jz} \mp \sqrt{3} \left(a^{\dagger}_{i\bar{z}} a_{jz} + a^{\dagger}_{iz} a_{j\bar{z}} \right) \right] - t \sum_{\langle ij\rangle \| c} a^{\dagger}_{iz} a_{jz}. \tag{11}$$

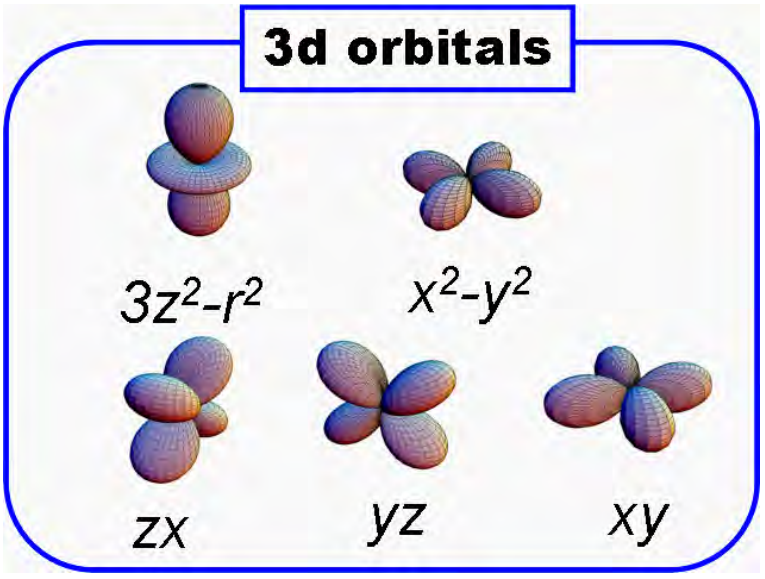

Fig. 4: *Schematic representation of* $3d$ *orbitals: Top—*e_g *orbital basis* $\{|3z^2{-}r^2\rangle, |x^2{-}y^2\rangle\}$. *Bottom—three* t_{2g} *orbital states* $\{|zx\rangle, |yz\rangle, |xy\rangle\} \equiv \{|b\rangle, |a\rangle, |c\rangle\}$. *These representations are split in a regular octahedron [3]. Image by courtesy of Yoshinori Tokura.*

Although this expression is of course cubic invariant, it does not manifest this symmetry but takes a very different appearance depending on the bond direction.
However, the symmetry is better visible using the basis of *complex* e_g *orbitals* at each site i [21],

$$|i{+}\rangle = \tfrac{1}{\sqrt{2}}\big(|iz\rangle - \mathrm{i}\,|i\bar{z}\rangle\big), \qquad |i{-}\rangle = \tfrac{1}{\sqrt{2}}\big(|iz\rangle + \mathrm{i}\,|i\bar{z}\rangle\big), \tag{12}$$

standing for "up" and"down" pseudospin flavors, with the local pseudospin operators being defined as follows,

$$\tau_i^{+} \equiv c_{i+}^{\dagger}c_{i-}, \qquad \tau_i^{-} \equiv c_{i-}^{\dagger}c_{i+}, \qquad \tau_i^{z} \equiv \tfrac{1}{2}(c_{i+}^{\dagger}c_{i+} - c_{i-}^{\dagger}c_{i-}) = \tfrac{1}{2}(n_{i+}{-}n_{i-}). \tag{13}$$

The three directional $\{|i\zeta_\gamma\rangle\}$ and three planar $\{|i\xi_\gamma\rangle\}$ orbitals at site i, associated with the three cubic axes ($\gamma \in \{a, b, c\}$), are the real orbitals,

$$|i\zeta_\gamma\rangle = \tfrac{1}{\sqrt{2}}\left[e^{-\mathrm{i}\vartheta_\alpha/2}|i{+}\rangle + e^{+\mathrm{i}\vartheta_\alpha/2}|i{-}\rangle\right] = \cos(\vartheta_\alpha/2)|iz\rangle - \sin(\vartheta_\alpha/2)|i\bar{z}\rangle, \tag{14}$$

$$|i\xi_\gamma\rangle = \tfrac{1}{\sqrt{2}}\left[e^{-\mathrm{i}\vartheta_\alpha/2}|i{+}\rangle - e^{+\mathrm{i}\vartheta_\alpha/2}|i{-}\rangle\right] = \sin(\vartheta_\alpha/2)|iz\rangle + \cos(\vartheta_\alpha/2)|i\bar{z}\rangle, \tag{15}$$

with the phase factors $\vartheta_{ia} = -4\pi/3$, $\vartheta_{ib} = +4\pi/3$, and $\vartheta_{ic} = 0$, and thus correspond to the pseudospin lying in the equatorial plane and pointing in one of the three equilateral "cubic" directions defined by the angles $\{\vartheta_{i\alpha}\}$.
Using the above complex-orbital representation (12), we can write the *orbital Hubbard model* for e_g electrons with only one spin flavor $\sigma =\uparrow$ in a form similar to the spin Hubbard model,

$$\mathcal{H}_{e_g}^{\uparrow} = -\frac{t}{2}\sum_{\gamma}\sum_{\langle ij\rangle\|\gamma}\Big[\Big(a_{i+}^{\dagger}a_{j+}{+}a_{i-}^{\dagger}a_{j-}\Big){+}\gamma\Big(e^{-\mathrm{i}\chi_\gamma}a_{i+}^{\dagger}a_{j-}{+}e^{+\mathrm{i}\chi_\gamma}a_{i-}^{\dagger}a_{j+}\Big)\Big]{+}\bar{U}\sum_{m}n_{i+}n_{i-}, \tag{16}$$

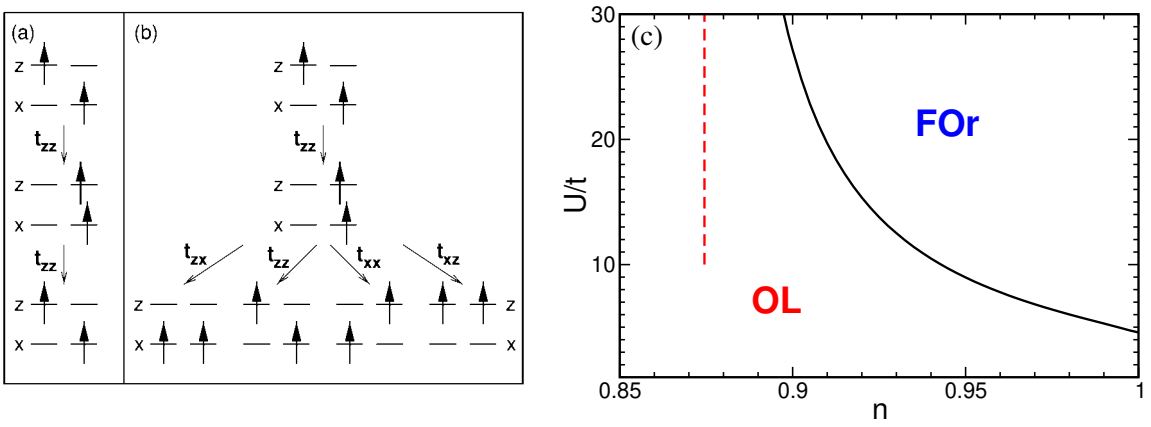

Fig. 5: *Virtual charge excitations leading to the e_g-orbital superexchange model for a strongly correlated system with $|z\rangle$ and $|x\rangle \equiv |\bar{z}\rangle$ real e_g orbitals (10) in the subspace of $\uparrow$-spin states: (a) for a bond along the c axis $\langle ij\rangle \parallel c$; (b) for a bond in the ab plane $\langle ij\rangle \parallel ab$. In a FM plane of $KCuF_3$ ($LaMnO_3$) the superexchange favors AO state of $|\mathrm{AO}\pm\rangle$ orbitals (not shown). (c) The transition from FOr to OL found at $d=\infty$ at finite U, and at $U=\infty$ (dashed line). Images (a-b) are reproduced from Ref. [22]; image (c) is reproduced from Ref. [23].*

with $\chi_a = +2\pi/3$, $\chi_b = -2\pi/3$, and $\chi_c = 0$, and where the parameter γ, explained below, takes for e_g orbitals the value $\gamma = 1$. The appearance of the phase factors $e^{\pm i\chi_\gamma}$ is characteristic of the orbital problem—these factors occur because the orbitals have an actual shape in real space so that each hopping process depends on the bond direction and may change the orbital flavor. The inter-orbital Coulomb interaction $\propto \bar{U}$ [22] is then the only Coulomb term which couples the electron densities in two basis orbitals $n_{i\mu} = a^\dagger_{i\mu}a_{i\mu}$, with $\mu \in \{+,-\}$; its form in invariant under any local basis transformation to a pair of orthogonal orbitals, i.e., it gives energy $\bar{U}$ for a double occupancy, either when two real orbitals are simultaneously occupied $\bar{U}n_{iz}n_{i\bar{z}}$, or when two complex orbitals are both occupied, $\bar{U}\sum_i n_{i+}n_{i-}$.

A charge excitation between two transition metal ions with partly filled e_g-orbitals will arise by a hopping process between two active orbitals, $|i\zeta_\gamma\rangle$ and $|j\zeta_\gamma\rangle$. To capture such processes we introduce two projection operators on the orbital states for each bond,

$$\mathcal{P}^{(\gamma)}_{\langle ij\rangle} \equiv \left(\frac{1}{2}+\tau^{(\gamma)}_i\right)\left(\frac{1}{2}-\tau^{(\gamma)}_j\right)+\left(\frac{1}{2}-\tau^{(\gamma)}_i\right)\left(\frac{1}{2}+\tau^{(\gamma)}_j\right), \tag{17}$$

$$\mathcal{Q}^{(\gamma)}_{\langle ij\rangle} \equiv 2\left(\frac{1}{2}-\tau^{(\gamma)}_i\right)\left(\frac{1}{2}-\tau^{(\gamma)}_j\right). \tag{18}$$

Recently a generalization of the e_g-orbital Hubbard model (16) was proposed to $d=\infty$ dimension [23]. Since the work of Metzner and Vollhardt [24] appeared, it is well known that the limit of $d=\infty$ is simpler for the correlation problems than any finite dimension as the diagrams addressing the correlations collapse to a single point and the Gutzwiller approximation to the variational ground state wave function [25] becomes exact [26]. The e_g orbital Hubbard model describes spinless fermions which propagate on a lattice and have two degenerate orbitals. Any double occupancy costs the same energy $\bar{U}$, exactly as in Eq. (16). A crucial observation is now that any orbital polarized state has no double occupancies, while the orbital liquid (OL) state has double occupancies and has to be renormalized.

The orbital Hubbard model (16) suggests that additional kinetic energy arises from the flavor-nonconserving hopping $\propto \gamma t$. Indeed, the only stable phase in the 3D e_g-orbital model is the orbital liquid (OL) phase [21]. In contrast, for the e_g-orbital model in $d = \infty$ dimensions [23], the OL dominates for most but not for all electron fillings. Indeed, close to half-filling $n = 1$, a FO phase is more stable. This phase has real e_g orbitals and is labeled as FOr in Fig. 5(c). Qualitatively this result is similar to the Nagaoka's theorem [27] for the spin Hubbard model, where a FM state is found close to half-filling. However, the mechanism is qualitatively different as the orbital-nonconserving hopping contributes and destabilizes the OL.
The resulting phase diagram of the e_g-orbital Hubbard model in the $(n, \bar{U})$ plane obtained in the Gutzwiller approximation contains mostly the OL phase, see Fig. 5(c). Here the FOr phase is more stable than the OL phase for $\bar{U} > U_c(n)$ if $n > n_c$. One finds the critical value $n_c = 0.8746$ of the electron density at which the energies of the OL and FOr are equal at $\bar{U} = \infty$, and below which the OL phase is therefore always stable.

3 Coulomb interactions in spin-orbital Hilbert space

3.1 Kanamori parameters: Coulomb U and Hund's exchange J

The full spin-orbital problem involves both degrees of freedom, as in Sec. 1. But in contrast to the simplified case of only one excitation energy U, one has to distinguish between different possible excitations, high-spin (HS) and low-spin (LS). Next to the Coulomb on-site repulsion U known from the Hubbard model, the degenerate Hubbard Hamiltonian [7] includes Hund's exchange J. In general, on-site Coulomb interactions between two electrons in $3d$ orbitals depend both on spin and orbital indices. Note that the electron interaction parameters in this model are effective ones, i.e., the $2p$-orbital parameters of O (or F) ions renormalize on-site Coulomb interactions between two electrons in $3d$ orbitals. A general form which includes only two-orbital interactions and the anisotropy of Coulomb and exchange elements is [28, 29]

$$\begin{aligned} H_{int} &= U \sum_{i\alpha} n_{i\alpha\uparrow} n_{i\alpha\downarrow} + \sum_{i,\alpha<\beta} \left(U'_{\alpha\beta} - \frac{1}{2} J_{\alpha\beta} \right) n_{i\alpha} n_{i\beta} - 2 \sum_{i,\alpha<\beta} J_{\alpha\beta}\, \vec{S}_{i\alpha} \cdot \vec{S}_{i\beta} \\ &+ \sum_{i,\alpha<\beta} J_{\alpha\beta} \left(a^{\dagger}_{i\alpha\uparrow} a^{\dagger}_{i\alpha\downarrow} a_{i\beta\downarrow} a_{i\beta\uparrow} + a^{\dagger}_{i\beta\uparrow} a^{\dagger}_{i\beta\downarrow} a_{i\alpha\downarrow} a_{i\alpha\uparrow} \right). \end{aligned} \tag{19}$$

Here $a^{\dagger}_{i\alpha\sigma}$ is an electron creation operator in any $3d$ orbital, $\alpha \in \{xy, yz, zx, 3z^2{-}r^2, x^2{-}y^2\}$, with spin states $\sigma = \uparrow, \downarrow$ at site i, and we shall use $\bar{\sigma} \equiv -\sigma$. The parameters $\{U, U'_{\alpha\beta}, J_{\alpha\beta}\}$ depend in general on the three Racah parameters $\{A, B, C\}$ [30], which may be derived from somewhat screened atomic values. While the intra-orbital Coulomb element is identical for all $3d$ orbitals,

$$U \equiv A + 4B + 3C, \tag{20}$$

the inter-orbital Coulomb $U'_{\alpha\beta}$ and exchange $J_{\alpha\beta}$ elements are anisotropic and depend on the involved pair of orbitals $\{\alpha, \beta\}$; the values of $J_{\alpha\beta}$ are given in Table 1. The inter-orbital Coulomb

Table 1: *On-site inter-orbital exchange elements $J_{\alpha\beta}$ for $3d$ orbitals as functions of the Racah parameters B and C (for more details see Ref. [30]).*

$3d$ orbital	xy	yz	zx	x^2-y^2	$3z^2-r^2$
xy	0	$3B+C$	$3B+C$	C	$4B+C$
yz	$3B+C$	0	$3B+C$	$3B+C$	$B+C$
zx	$3B+C$	$3B+C$	0	$3B+C$	$B+C$
x^2-y^2	C	$3B+C$	$3B+C$	0	$4B+C$
$3z^2-r^2$	$4B+C$	$B+C$	$B+C$	$4B+C$	0

$U'_{\alpha\beta}$ and Hund's exchange $J_{\alpha\beta}$ elements satisfy a relation with intra-orbital element U which guarantees the rotational invariance of interactions in the orbital space,

$$U = U'_{\alpha\beta} + 2J_{\alpha\beta}. \tag{21}$$

In all situations where only the orbitals belonging to a single irreducible representation of the cubic group (e_g or t_{2g}) are partly filled, e.g. in the titanates, vanadates, nickelates, or copper fluorides, the filled (empty) orbitals do not contribute to the dynamics, and the relevant exchange elements $J_{\alpha\beta}$ are all the same (see Table 1), i.e., either a pair of t_{2g} or for e_g orbitals,

$$J_H^t \equiv 3B+C, \tag{22}$$

$$J_H^e \equiv 4B+C. \tag{23}$$

Then one may use a simplified *degenerate* Hubbard model [7] with isotropic on-site interactions (for a given subset of $3d$ orbitals),

$$\begin{aligned} H_{int}^{(0)} &= U\sum_{i\alpha} n_{i\alpha\uparrow}n_{i\alpha\downarrow} + \left(U-\frac{5}{2}J_H\right)\sum_{i,\alpha<\beta} n_{i\alpha}n_{i\beta} - 2J_H\sum_{i,\alpha<\beta}\vec{S}_{i\alpha}\cdot\vec{S}_{i\beta} \\ &+J_H\sum_{i,\alpha<\beta}\left(a^\dagger_{i\alpha\uparrow}a^\dagger_{i\alpha\downarrow}a_{i\beta\downarrow}a_{i\beta\uparrow} + a^\dagger_{i\beta\uparrow}a^\dagger_{i\beta\downarrow}a_{i\alpha\downarrow}a_{i\alpha\uparrow}\right). \end{aligned} \tag{24}$$

Eq. (24) has two Kanamori parameters: the Coulomb intra-orbital element U (20) and Hund's exchange J_H, and we parametrize the interactions by

$$\eta = J_H/U \tag{25}$$

which stands either for J_H^t (22) or for J_H^e (23), depending on the electronic filling of $3d$ orbitals at site i. Here we also obtain the celebrated element $\bar{U} \equiv U-3J_H^e$, used before in Eq. (16) when only HS states occur. We emphasize that in a general case when both types of orbitals are partly filled, as in the colossal magnetoresistance (CMR) manganites [31], and both thus participate in charge excitations of Fig. 6, the above Hamiltonian with a single Hund's exchange element J_H^e is insufficient and the full anisotropy given in Eq. (24) has to be used instead to generate the correct charge excitation spectra for a given transition metal ion [30].

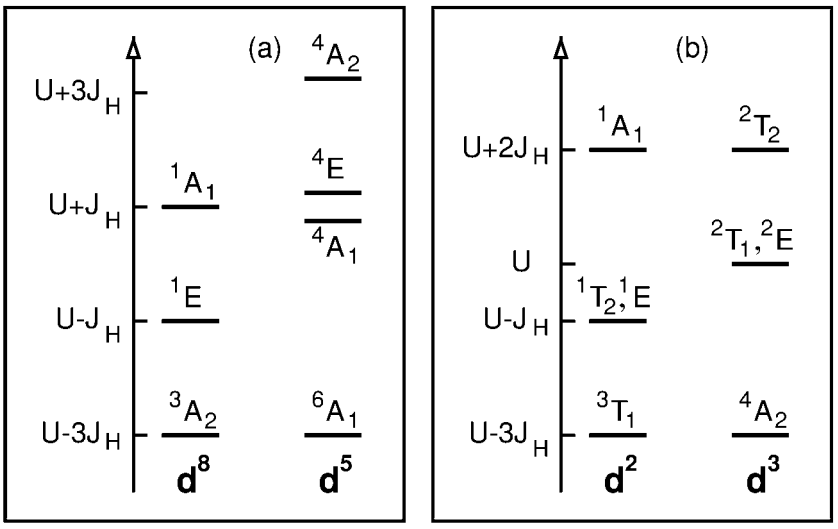

Fig. 6: *Energies of charge excitations ε_n (26) for selected cubic transition metal oxides, for: (a) e_g excitations to Cu^{3+} (d^8) and Mn^{2+} (d^5) ions; (b) t_{2g} excitations to Ti^{2+} (d^2) and V^{2+} (d^3) ions. The splittings between different states are due to Hund's exchange element J_H which refers to a pair of e_g and t_{2g} electrons in (a) and (b). Image reproduced from Ref. [28].*

In a strongly correlated regime $t \ll U$, we consider the case of partly filled degenerate $3d$ orbitals and large Hund's exchange J_H. This guarantees that electrons localize in high-spin ionic states, and effective low-energy superexchange interactions consist of all the contributions which originate from possible virtual charge excitations, $d_m^p d_n^p \rightleftharpoons d_m^{p+1} d_n^{p-1}$ —they take the form of a spin-orbital model. The charge excitation n costs the energy

$$\varepsilon_n = E_n(d^{p+1}) + E_0(d^{p-1}) - 2E_0(d^p), \tag{26}$$

where the d^p ions are in the initial high-spin ground states with spins $S = \frac{p}{2}$ and have the Coulomb interaction energy $E_0(d^p) = \binom{p}{2}(U - 3J_H^e)$ each if $p < 5$ (otherwise if $p > 5$ one has to consider p holes instead). The case of $p = 5$ electrons is special and will not be considered here as in the $t_{2g}^3 e_g^2$ configuration the orbital degree of freedom is quenched.

The same formula for the ground state energy applies as well to Mn^{3+} ions in d^4 configuration with $S = 2$ spin HS ground state, see Sec. 2. By construction, also the ion with less electrons (holes) for $p < 5$ ($p > 5$) is in the HS state and $E_0(d^{p-1}) = \binom{p-1}{2}(U - 3J_H)$. The excitation energies (26) are thus defined by the multiplet structure of an ion with more electrons (holes) in the configuration d^{p+1}, see Fig. 6. The lowest energy excitation is always given by $U - 3J_H$ —it is obtained from the HS state of the $3d^{p+1}$ ion with total spin $\mathcal{S} = S + 1/2$ and energy $E_1(d^{p+1}) = \binom{p+1}{2}(U - 3J_H)$, with J_H being Hund's exchange element for the electron (hole) involved in the charge excitation, either e_g or t_{2g}. Indeed, one recovers the lowest excitation energy in the HS subspace, ε_1. We emphasize that this lowest excitation energy ε_1 is universal and is found both in t_{2g} and e_g subspaces, i.e., it does not depend on the electron valence p, see Fig. 6. In contrast, the remaining energies $\{\varepsilon_n\}$ for $n > 1$ are all for LS excitations and are specific to a given valence p of the considered insulator with d^p ions. They have to be determined from the full local Coulomb interaction Hamiltonian (19), in general including also the anisotropy of the $\{U_{\alpha\beta}\}$ and $\{J_{\alpha\beta}\}$ elements.

Effective interactions in a Mott (or charge transfer) insulator with orbital degeneracy take the form of spin-orbital superexchange [1, 12]. Its general structure is given by the sum over all the nearest neighboring bonds $\langle ij\rangle \parallel \gamma$ connecting two transition metal ions and over the excitations n possible for each of them as,

$$\mathcal{H} = -\sum_n \frac{t^2}{\varepsilon_n} \sum_{\langle ij\rangle\parallel\gamma} P_{\langle ij\rangle}(\mathcal{S})\, \mathcal{O}^{\gamma}_{\langle ij\rangle}, \tag{27}$$

where $P_{\langle ij\rangle}(\mathcal{S})$ is the projection on the total spin $\mathcal{S} = S \pm 1/2$ and $\mathcal{O}^{\gamma}_{\langle ij\rangle}$ is the projection operator on the orbital state at the sites i and j of a given bond. Following this general procedure, one finds a spin-orbital model with Heisenberg spin interactions for spins $S = {}^{p}/_{2}$ of SU(2) symmetry coupled to the orbital operators which have much lower cubic symmetry, with the general structure of spin-orbital superexchange $\propto J$ (2) [28],

$$\mathcal{H}_J = J \sum_{\gamma} \sum_{\langle ij\rangle\parallel\gamma} \left\{ \hat{\mathcal{K}}^{(\gamma)}_{ij} \left(\vec{S}_i \cdot \vec{S}_j + S^2 \right) + \hat{\mathcal{N}}^{(\gamma)}_{ij} \right\}. \tag{28}$$

It connects ions at sites i and j along the bond $\langle ij\rangle \parallel \gamma$ and involves orbital operators, $\hat{\mathcal{K}}^{(\gamma)}_{ij}$ and $\hat{\mathcal{N}}^{(\gamma)}_{ij}$, which depend on the bond direction $\gamma = a, b, c$ for the three *a priori* equivalent directions in a cubic crystal. The spin scalar product, $\vec{S}_i \cdot \vec{S}_j$, is coupled to orbital operators $\hat{\mathcal{K}}^{(\gamma)}_{ij}$ which together with the other "decoupled" orbital operators, $\hat{\mathcal{N}}^{(\gamma)}_{ij}$, determine the orbital state in a Mott insulator. The form of these operators depends on the type of orbital degrees of freedom in a given model. They involve active orbitals on each bond $\langle ij\rangle \parallel \gamma$ along direction γ. Thus the orbital interactions are directional and have only the cubic symmetry of a (perovskite) lattice provided the symmetry in the orbital sector is not broken by other interactions, for instance by CF or Jahn-Teller (JT) terms.

The magnetic superexchange constants along each cubic axis J_{ab} and J_c in the effective spin model,

$$H = J_{ab} \sum_{\langle ij\rangle\parallel ab} \vec{S}_i \cdot \vec{S}_j + J_c \sum_{\langle ij\rangle\parallel c} \vec{S}_i \cdot \vec{S}_j, \tag{29}$$

are obtained from the spin-orbital model (28) by decoupling spin and orbital operators and next averaging the orbital operators over an underlying orbital (ordered or disordered) state. It gives effective magnetic exchange interactions: J_c for a bond along the c axis, and J_{ab} for bonds within the ab plane. The latter ones J_{ab}, could in principle still be different between the a and b axes in case of finite lattice distortions due to the JT effect or octahedra tilting, but we limit ourselves to idealized structures, with J_{ab} being the same for both planar directions. We show below that the spin-spin correlations along the c axis and within the ab planes,

$$s_c = \left\langle \vec{S}_i \cdot \vec{S}_j \right\rangle_c, \qquad s_{ab} = \left\langle \vec{S}_i \cdot \vec{S}_j \right\rangle_{ab}, \tag{30}$$

next to the orbital correlations, play an important role in the intensity distribution in optical spectroscopy.

In correlated insulators with partly occupied degenerate orbitals, not only the structure of the superexchange (28) is complex, but also the optical spectra exhibit strong anisotropy and temperature dependence near the magnetic transitions, as found, e.g., in $LaMnO_3$ [32, 33] or in the cubic vanadates, $LaVO_3$ and YVO_3 [28]. In such systems several excitations contribute to the excitation spectra, so one may ask how the spectral weight redistributes between individual subbands originating from these excitations. The spectral weight distribution is in general anisotropic already when orbital order (OO) [34] sets in and breaks the cubic symmetry, but even more so when A-type or C-type AF spin order occurs below the Néel temperature $T_{\rm N}$. At orbital degeneracy the superexchange consists of the terms $\propto H_n^{(\gamma)}(ij)$ as a superposition of individual contributions on each bond $\langle ij\rangle$ due to charge excitation n (26) [35],

$$\mathcal{H} = J \sum_n \sum_{\langle ij\rangle \| \gamma} H_n^{(\gamma)}(ij), \tag{31}$$

with the energy unit for each individual $H_n^{(\gamma)}(ij)$ term given by the superexchange constant J, see Eq. (2). It follows from d-d charge excitations with an effective hopping element t between neighboring transition metal ions and is the same as that obtained in a Mott insulator with nondegenerate orbitals in the regime of $U \gg t$. The spectral weight in optical spectroscopy is determined by the kinetic energy, and reflects the onset of spin order (SO) and/or OO [35]. In a correlated insulator, electrons are almost localized and the only kinetic energy which is left is associated with the same virtual charge excitations that contribute also to the superexchange. Therefore, the individual kinetic energy terms $K_n^{(\gamma)}$ may be directly determined from the superexchange (31) using the Hellmann-Feynman theorem,

$$K_n^{(\gamma)} = -2J \left\langle H_n^{(\gamma)}(ij) \right\rangle . \tag{32}$$

For convenience, we define here the $K_n^{(\gamma)}$ as positive quantities. Each term $K_n^{(\gamma)}$ (32) originates from a given charge excitation n along a bond direction $\langle ij\rangle \parallel \gamma$. These terms are straightforwardly related to the *partial optical sum rule* for individual Hubbard subbands, which reads [35]

$$\frac{a_0 \hbar^2}{e^2} \int_0^\infty \sigma_n^{(\gamma)}(\omega)\, d\omega = \frac{\pi}{2} K_n^{(\gamma)}, \tag{33}$$

where $\sigma_n^{(\gamma)}(\omega)$ is the contribution of excitation n to the optical conductivity for polarization along the γ axis, a_0 is the distance between transition metal ions, and the tight-binding model with nearest neighbor hopping is implied. Using Eq. (32) one finds that the intensity of each band is indeed determined by the underlying OO together with the spin-spin correlation along the direction corresponding to the polarization.

One has to distinguish the above partial sum rule (33) from the full sum rule for the total spectral weight in the optical spectroscopy for polarization along a cubic direction γ, involving

$$K^{(\gamma)} = -2J \sum_n \left\langle H_n^{(\gamma)}(ij) \right\rangle , \tag{34}$$

which stands for the total intensity in the optical d-d excitations. This quantity is usually of less interest as it does not allow for a direct insight into the nature of the electronic structure

being a sum over several excitations ε_n (26) and has a much weaker temperature dependence. In addition, it might also be more difficult to deduce the quantity from experiment.

3.2 Goodenough-Kanamori rules

While a rather advanced treatment of the quantum many-body physics is required in general for spin-orbital models, we want to present here certain principles which help to understand the heart of the problem and to give simple guidelines for interpreting experiments and for finding relevant physical parameters of the spin-orbital models of *undoped* cubic insulators. We will argue that such an approach based upon classical OO is well justified in many known cases, as quantum phenomena are often quenched by the JT coupling between orbitals and by lattice distortions, which are present below structural phase transitions and induce OO, either in spin-disordered, in spin-ordered phases, or in spin-liquid.

From the derivation of the Kugel-Khomskii (KK) model in Sec. 4.1, we observe that pairs of directional orbitals $\{|i\zeta_\gamma\rangle, |j\zeta_\gamma\rangle\}$ on neighboring ions favor AF SO, while pairs of orthogonal orbitals such as $\{|i\zeta_\gamma\rangle, |j\xi_\gamma\rangle\}$ favor FM SO. This is known as classical Goodenough-Kanamori rules (GKR) [36] predicting that the state with AF SO has simultaneously FO order, while FM SO is accompanied by AO order, see Figs. 7(a) and 7(b). Indeed, these rules emphasizing the complementarity of spin-orbital correlations are frequently employed to explain the observed spin-orbital order in several systems, particularly in those where spins are large, like in CMR manganites [31]. They agree with the general structure of spin-orbital superexchange in the KK model, where it is sufficient to consider the flavor-conserving hopping between pairs of directional orbitals $\{|i\zeta_\gamma\rangle, |j\zeta_\gamma\rangle\}$ [29, 37]. The excited states are then doubly occupied in one of the directional orbitals, while no effective interaction arises for two parallel spins (in triplet states), so the superexchange is AF. In contrast, for a pair of orthogonal orbitals, e.g. $\{|i\zeta_\gamma\rangle, |j\xi_\gamma\rangle\}$, two different orbitals are singly occupied and the FM term is stronger than the AF one as the excitation energy is lower. Therefore, configurations with AO order support FM SO.

The above complementarity of spin-orbital order is frustrated by inter-orbital hopping, or may be modified by spin-orbital entanglement [11], see below. In such cases the order in both channels could be the same, either FM/FO, see Fig. 7(c), or AF/AO, see Fig. 7(d). Again, when different orbitals are occupied in the excited state, the spin superexchange is weakly FM and when the same orbital is doubly occupied, the spin superexchange is stronger and AF. The latter AF exchange coupling dominates because antiferromagnetism, which is due to the Pauli principle, does not have to compete here with ferromagnetism. On the contrary, FM exchange is caused by the energy difference $\propto \eta$ between triplet and singlet excited states, with two different orbitals occupied.

This modification of the GKR is of importance in alkali RO_2 hyperoxides ($R =$ K, Rb, Cs) [38]. The JT effect is crucial for this generalization of the GKR—without it large inter-orbital hopping orders the T^x-orbital-mixing pseudospin component instead of the T^z component in a single plane. Altogether, such generalized GKR can arise whenever the OO on a bond is not solely stabilized by the same spin-orbital superexchange interaction that determines the spin exchange.

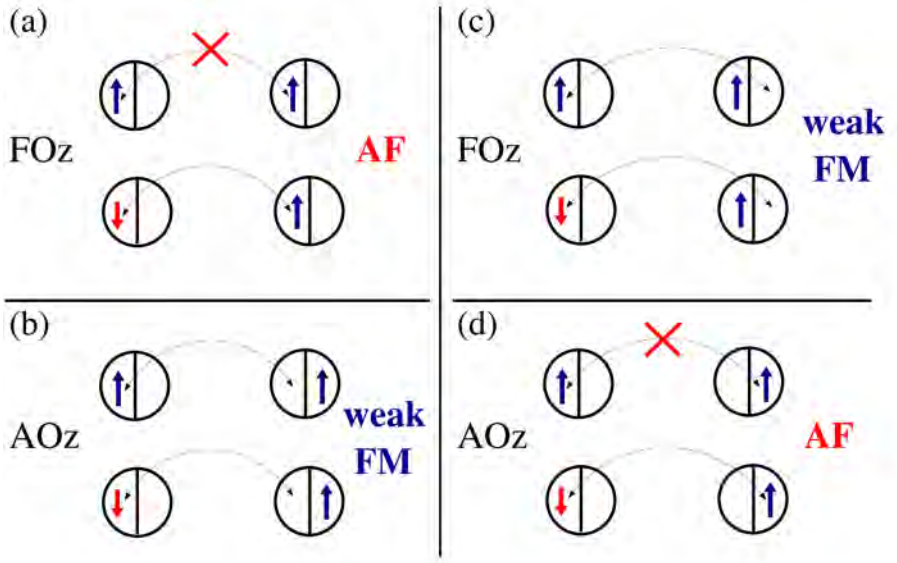

Fig. 7: *Artist's view of the GKR [36] for: (a) FOz and AF spin order and (b) AOz and FM spin order in a system with orbital flavor conserving hopping as alkali RO_2 hyperoxides (R = K, Rb, Cs) [38]. The charge excitations generated by inter-orbital hopping fully violate the GKR and support the states with the same spin-orbital order: (c) FOz and FM spin order and (d) AOz and AF spin order. Image reproduced from Ref. [38].*

On a geometrically frustrated lattice, for instance, another route to this behavior can occur when the ordered orbital component preferred by superexchange depends on the direction and the relative strengths fulfill certain criteria.

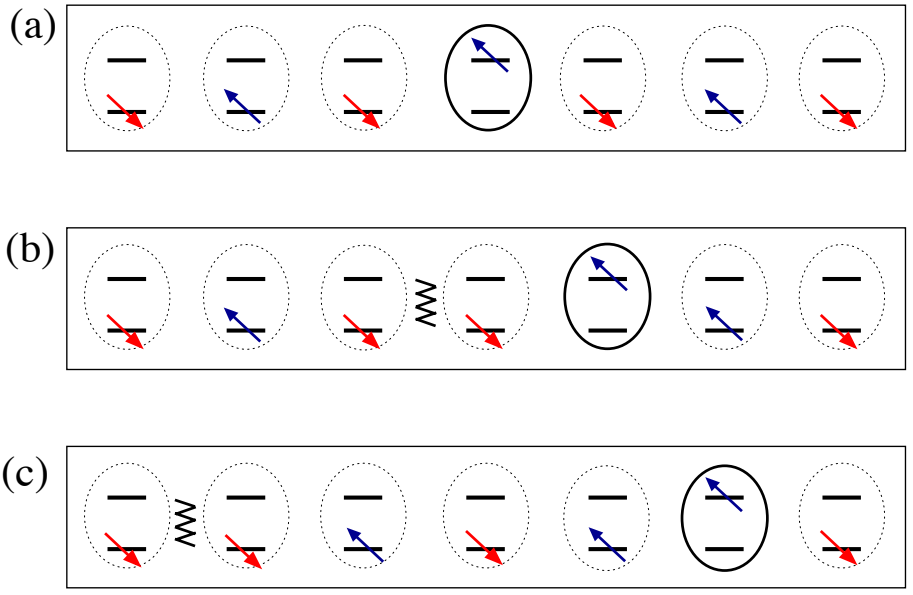

Fig. 8: *Schematic representation of the orbital motion and the spin-orbital separation in a 1D spin-orbital model. The first hop of the excited state (a)→(b) creates a spinon (wavy line) that moves via spin exchange $\propto J$. The next hop (b)→(c) gives an "orbiton" freely propagating as a "holon" with an effective hopping $t \sim J/2$. Image reproduced from Ref. [39].*

While a hole doped to the FM chain propagates freely, it creates a spinon and a holon in an AF background described by the t-J model. A similar situation occurs for an orbital excitation in an AF/FO spin-orbital chain [39]. An orbital excitation may propagate through the system only after creating a spinon in the first step, see Figs. 8(a) and 8(b). The spinon itself moves via spin flips $\propto J > t$, faster than the orbiton, and the two excitations get well separated, see Fig. 8(c). The orbital-wave picture of Sec. 2, on the other hand, would require the orbital excitation to move without creating the spinon in the first step. Note that this would be only possible for imperfect Néel AF SO. Thus, one concludes that the symmetry between spin and orbital sector is broken also for this reason and orbitals are so strongly coupled to spin excitations in realistic spin-orbital models with AF/FO order. In conclusion the mean field picture separating these two sectors of the Hilbert space breaks down.

4 Kugel-Khomskii model for Mott insulators

4.1 Kugel-Khomskii model: 3D for $KCuF_3$ and 2D for K_2CuF_4

The simplest and seminal spin-orbital model is obtained when a fermion has two flavors, spin and orbital, and both have two components, i.e., spin and pseudospin are $S = T = 1/2$. The physical realization is found in cuprates with degenerate e_g orbitals, such as $KCuF_3$ or K_2CuF_4 [1], where Cu^{2+} ions are in the d^9 electronic configuration, so charge excitations $d_i^9 d_j^9 \rightleftharpoons d_i^{10} d_j^8$ are made by holes. By considering the degenerate Hubbard model for two e_g orbitals one finds that d^8 ions have an equidistant multiplet structure, with three excitation energies which differ by $2J_H$ [here J_H stands for the J_H^e given by Eq. (23)], see Table 2. We emphasize that the correct spectrum has a doubly degenerate energy $U-J_H$, and the highest non-degenerate energy is $U+J_H$, see Fig. 6(a). Note that this result follows from the diagonalization of the local Coulomb interactions in the relevant subspaces—it reflects the fact that a double occupancy $\big(|z\uparrow z\downarrow\rangle$ or $|\bar{z}\uparrow\bar{z}\downarrow\rangle\big)$ in either orbital state ($|z\rangle$ or $|\bar{z}\rangle$) is not an eigenstate of the degenerate Hubbard model in the atomic limit (24), so the excitation energy U is absent in the spectrum, see Table 2.
The total spin state on the bond $\langle ij\rangle$ corresponds to $\mathcal{S}$=1 or 0, so the spin projection operators $P_{\langle ij\rangle}(1)$ and $P_{\langle ij\rangle}(0)$ are easily deduced, see Table 2. The orbital configuration on a bond $\langle ij\rangle$ is given by one of the orbital operators in Sec. 2, either $\mathcal{P}^{(\gamma)}_{\langle ij\rangle}$ for the doubly occupied states involving different orbitals, or $\mathcal{Q}^{(\gamma)}_{\langle ij\rangle}$ for a double occupancy in a directional orbital at site i or j. This gives the rather transparent structure of one HS and three LS excitations in Table 2. The 3D KK model then follows from Eq. (27) [9,40]:

$$\mathcal{H}(d^9) = \sum_{\gamma}\sum_{\langle ij\rangle\parallel\gamma}\left\{-\frac{t^2}{U-3J_H}\left(\vec{S}_i\cdot\vec{S}_j+\frac{3}{4}\right)\mathcal{P}^{(\gamma)}_{\langle ij\rangle}+\frac{t^2}{U-J_H}\left(\vec{S}_i\cdot\vec{S}_j-\frac{1}{4}\right)\mathcal{P}^{(\gamma)}_{\langle ij\rangle}\right.$$
$$\left.+\left(\frac{t^2}{U-J_H}+\frac{t^2}{U+J_H}\right)\left(\vec{S}_i\cdot\vec{S}_j-\frac{1}{4}\right)\mathcal{Q}^{(\gamma)}_{\langle ij\rangle}\right\}+E_z\sum_i\tau_i^{(c)}. \quad (35)$$

The last term $\propto E_z$ is the CF which splits off the degenerate e_g orbitals when a JT lattice distortion occurs, and is together with Hund's exchange η, a second parameter to construct

Table 2: *Elements needed for the construction of the KK model from charge excitations on the bond $\langle ij\rangle$: excitation n, its type (HS or LS) and energy ε_n, total spin state (triplet or singlet) and the spin projection operator $P_{\langle ij\rangle}(\mathcal{S})$, and the orbital state and the corresponding orbital projection operator.*

charge excitation			spin state		orbital state	orbital
n	type	ε_n	$\mathcal{S}$	$P_{\langle ij\rangle}$	on a bond $\langle ij\rangle \parallel \gamma$	projection
1	HS	$U-3J_H$	1	$\left(\vec{S}_i\cdot\vec{S}_j+\frac{3}{4}\right)$	$\vert i\zeta_\gamma\rangle\vert j\xi_\gamma\rangle$ $(\vert i\xi_\gamma\rangle\vert j\zeta_\gamma\rangle)$	$\mathcal{P}^{(\gamma)}_{\langle ij\rangle}$
2	LS	$U-J_H$	0	$-\left(\vec{S}_i\cdot\vec{S}_j-\frac{1}{4}\right)$	$\vert i\zeta_\gamma\rangle\vert j\xi_\gamma\rangle$ $(\vert i\xi_\gamma\rangle\vert j\zeta_\gamma\rangle)$	$\mathcal{P}^{(\gamma)}_{\langle ij\rangle}$
3	LS	$U-J_H$	0	$-\left(\vec{S}_i\cdot\vec{S}_j-\frac{1}{4}\right)$	$\vert i\zeta_\gamma\rangle\vert j\zeta_\gamma\rangle$	$\mathcal{Q}^{(\gamma)}_{\langle ij\rangle}$
4	LS	$U+J_H$	0	$-\left(\vec{S}_i\cdot\vec{S}_j-\frac{1}{4}\right)$	$\vert i\zeta_\gamma\rangle\vert j\zeta_\gamma\rangle$	$\mathcal{Q}^{(\gamma)}_{\langle ij\rangle}$

phase diagrams, see below. Here it refers to holes, i.e., large $E_z>0$ favors hole occupation in $|\bar{z}\rangle\equiv|x^2{-}y^2\rangle/\sqrt{2}$ orbitals, as in La_2CuO_4. On the other hand, while $E_z\simeq 0$, both orbitals have almost equal hole (electron) density.

Another form of the Hamiltonian (35) is obtained by introducing the coefficients,

$$r_1=\frac{1}{1{-}3\eta},\qquad r_2=r_3=\frac{1}{1{-}\eta},\qquad r_4=\frac{1}{1{+}\eta}, \tag{36}$$

and defining the superexchange constant J in the same way as in the t-J model Eq. (2). With the explicit representation of the orbital operators $\mathcal{P}^{(\gamma)}_{\langle ij\rangle}$ and $\mathcal{Q}^{(\gamma)}_{\langle ij\rangle}$ in terms of $\left\{\tau_i^{(\gamma)}\right\}$ one finds,

$$\begin{aligned}\mathcal{H}(d^9) \;=\; \frac{1}{2}J\sum_\gamma\sum_{\langle ij\rangle\parallel\gamma}\Bigg\{&\left[-r_1\left(\vec{S}_i\cdot\vec{S}_j+\frac{3}{4}\right)+r_2\left(\vec{S}_i\cdot\vec{S}_j-\frac{1}{4}\right)\right]\left(\frac{1}{4}-\tau_i^{(\gamma)}\tau_j^{(\gamma)}\right)\\&+(r_3{+}r_4)\left(\vec{S}_i\cdot\vec{S}_j-\frac{1}{4}\right)\left(\tau_i^{(\gamma)}+\frac{1}{2}\right)\left(\tau_j^{(\gamma)}+\frac{1}{2}\right)\Bigg\}+E_z\sum_i\tau_i^{(c)}.\end{aligned} \tag{37}$$

In the FM state spins are integrated out and one finds from the first term just the superexchange in the e_g orbital model analyzed above in Sec. 2.

The magnetic superexchange constants J_{ab} and J_c employed in the effective spin-orbital model (37) are obtained by decoupling spin and orbital operators and next averaging the orbital operators $\left\langle\hat{\mathcal{K}}_{ij}^{(\gamma)}\right\rangle$ over the classical state $|\Phi_0\rangle$ as given by Eq. (12). The relevant averages are given in Table 3, and they lead to the following expressions for the superexchange constants in Eq. (29),

$$J_c \;=\; \frac{1}{8}J\Big\{-r_1\sin^2\theta+(r_2{+}r_3)(1+\cos\theta)+r_4(1+\cos\theta)^2\Big\}, \tag{38}$$

$$J_{ab} \;=\; \frac{1}{8}J\left\{-r_1\left(\frac{3}{4}+\sin^2\theta\right)+(r_2{+}r_3)\left(1-\frac{1}{2}\cos\theta\right)+r_4\left(\frac{1}{2}-\cos\theta\right)^2\right\}, \tag{39}$$

which depend on two parameters: J from Eq. (2) and η as in Eq. (25), as well as on the OO of $|\pm\rangle$ orbitals specified by the orbital angle θ. It is clear that the FM term $\propto r_1$ competes

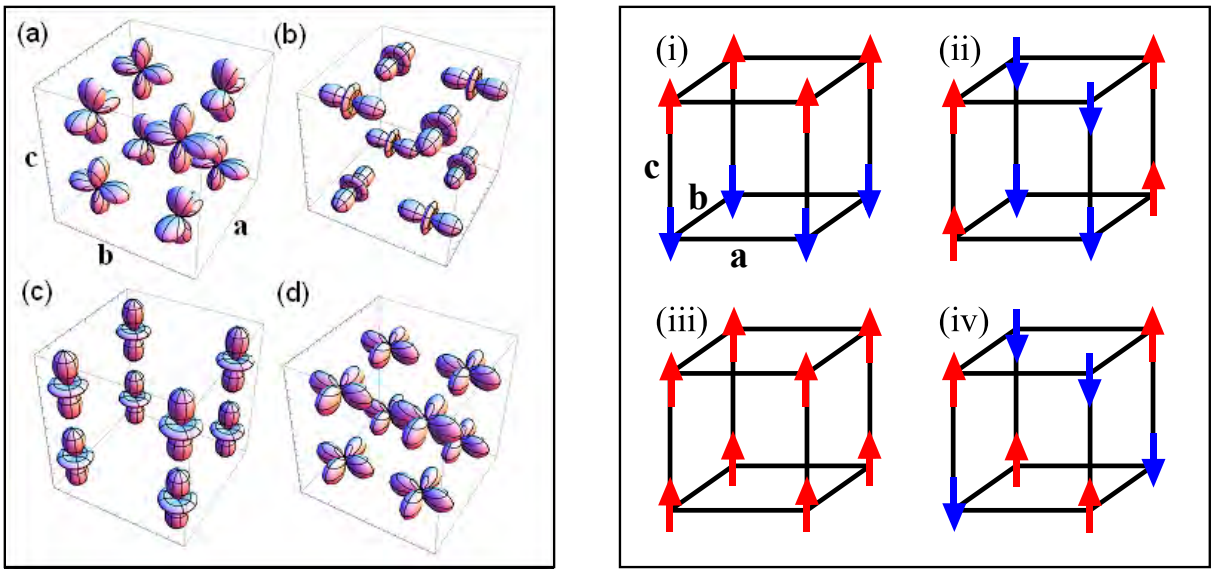

Fig. 9: *Spin-orbital entanglement in the KK model includes orbitals and spins: Left—schematic view of the four simplest e_g-orbital configurations on a representative cube of the 3D lattice: (a) alternating orbital (AO) order with $\langle\tau_i^{(a,b)}\rangle=\pm 1/2$ changing from site to site, and $\langle\tau_i^{c}\rangle=1/4$, obtained for $E_z<0$, (b) AO order with $\langle\tau_i^{(a,b)}\rangle=-1/2$, alternating between sites and $\langle\tau_i^{(c)}\rangle=-1/4$, obtained for $E_z>0$, (c) FO order with occupied z orbitals and $\langle\tau_i^{c}\rangle=1/2$ (cigar-shaped orbitals), and (d) FO order with occupied $\bar{z}$ orbitals and $\langle\tau_i^{c}\rangle=-1/2$ (clover-shaped orbitals). Right—schematic view of four spin configurations (arrows for up or down spins; $\{a,b,c\}$ are crystallographic directions) in phases with SO: (i) A-AF, (ii) C-AF, (iii) FM, and (iv) G-AF. Image by courtesy of Wojciech Brzezicki.*

with all the other AF LS terms. Nevertheless, in the ab planes, where the occupied hole e_g orbitals alternate, the larger FM contribution dominates and makes the magnetic superexchange J_{ab} weakly FM ($J_{ab}\lesssim 0$ when $\sin^2\theta\simeq 1$), while the stronger AF superexchange along the c axis ($J_c\gg|J_{ab}|$) favors quasi one-dimensional (1D) spin fluctuations. Thus $KCuF_3$ exhibits spinon excitations for $T>T_{\rm N}$.

Table 3: *Averages of the orbital projection operators standing in the spin-orbital interactions in the KK model (37) and determine the spin interactions in H_s (29) for the C-type OO of occupied e_g orbitals which alternate in the ab planes, as given by Eqs. (14). Nonequivalent cubic directions along the $\langle ij\rangle$ bonds are labeled by $\gamma=ab,c$.*

operator	average	ab	c
$\mathcal{Q}_{\langle ij\rangle}^{(\gamma)}$	$2\left\langle\left(\frac{1}{2}-\tau_i^{(\gamma)}\right)\left(\frac{1}{2}-\tau_j^{(\gamma)}\right)\right\rangle$	$\frac{1}{2}\left(\frac{1}{2}-\cos\theta\right)^2$	$\frac{1}{2}\left(1+\cos\theta\right)^2$
$\mathcal{P}_{\langle ij\rangle}^{(\gamma)}$	$\left\langle\frac{1}{4}-\tau_i^{(\gamma)}\tau_j^{(\gamma)}\right\rangle$	$\frac{1}{4}\left(\frac{3}{4}+\sin^2\theta\right)$	$\frac{1}{4}\sin^2\theta$
$\mathcal{R}_{\langle ij\rangle}^{(\gamma)}$	$2\left\langle\left(\frac{1}{2}+\tau_i^{(\gamma)}\right)\left(\frac{1}{2}+\tau_j^{(\gamma)}\right)\right\rangle$	$\frac{1}{2}\left(\frac{1}{2}+\cos\theta\right)^2$	$\frac{1}{2}\left(1-\cos\theta\right)^2$

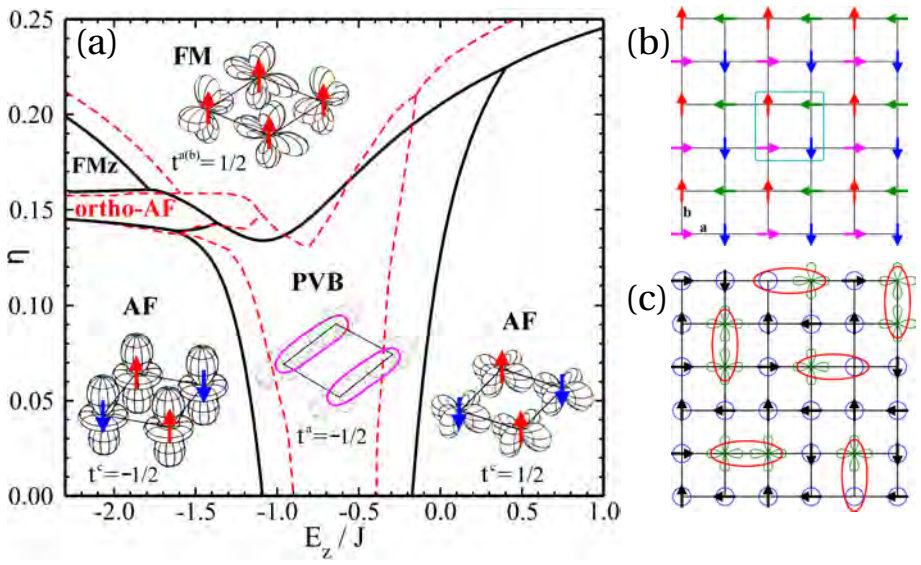

Fig. 10: *Spin-orbital phase diagram and entanglement in the 2D KK model: (a) phase diagram in the plaquette mean field (solid lines) and ERA (dashed lines) variational approximation, with insets showing representative spin and orbital configurations on a 2×2 plaquette—$\bar{z}$-like $\left(t^c{=}-\langle\tau_i^{(c)}\rangle{=}\frac{1}{2}\right)$ and z-like $\left(t^{a,c}{=}-\langle\tau_i^{(c,a)}\rangle{=}-\frac{1}{2}\right)$ orbitals are accompanied either by AF long range spin order (arrows) or by spin singlets on bonds in the PVB phase (ovals); (b) view of an exotic four-sublattice ortho-AF phase near the onset of FM (or FMz) phase; (c) artist's view of the ortho-AF phase—spin singlets (ovals) are entangled with either one or two orbital excitations $|z\rangle \rightarrow |\bar{z}\rangle$ (clovers). Images reproduced from Ref. [41].*

Consider first the 2D KK model on a square lattice, with $\gamma = a, b$ in Eq. (37), as in K_2CuF_4. In the absence of Hund's exchange, interactions between $S = {}^1/_2$ spins are AF. However, they are quite different depending on which of the two e_g orbitals are occupied by holes: $J^z_{ab} = \frac{1}{16}J$ for $|z\rangle$ and $J^{\bar{z}}_{ab} = \frac{9}{16}J$ for $|\bar{z}\rangle$ hole orbitals. As a result, the AF phases with SO in Fig. 9(iv) and the FO order shown in Figs. 9(c) and 9(d) are degenerate at finite CF $E_z = -\frac{1}{2}J$. This defines a quantum critical point (QCP) $Q_{2D} = (-{}^1/_2, 0)$ in the $(E_z/J, \eta)$ plane [while $Q_{3D} = (0, 0)$]. Actually, at this point also one more phase has the same energy—the FM spin phase of Fig. 9(i) with AO order of $|\pm\rangle$ orbitals, shown in Figs. 5(a&b) [40].

To capture the corrections due to quantum fluctuations, one may construct a plaquette mean field approximation or entanglement renormalization *ansatz* (ERA) [41]. One finds important corrections to the mean field phase diagram near the QCP Q_{2D}, and a plaquette valence bond (PVB) state is stable in between the above three phases accompanied by spin-orbital long range order, with spin singlets on the bonds $\parallel a$ ($\parallel b$) and stabilized by the directional orbitals $|\zeta_a\rangle$ ($|\zeta_b\rangle$). A novel ortho-AF phase appears as well when the magnetic interactions change from AF to FM ones due to increasing Hund's exchange η, and for $E_z/J < -1.5$, see Fig. 10(a). Since the nearest neighbor magnetic interactions are very weak, exotic four-sublattice ortho-AF SO emerges due to second and third nearest neighbor interactions, shown in Fig. 10(b). Such further neighbor interactions follow from spin-orbital excitations shown in Fig. 10(c). Note that both approximate methods employed in Ref. [41] (plaquette mean field approximation and ERA) give very similar range of stability of the ortho-AF phase.

4.2 Entanglement in the ferromagnetic excitations of K_2CuF_4

To investigate magnons (spin waves), we create a spin excitation at site $i = 0$ by decreasing the value of the order parameter $\langle S_0^z \rangle$ from S to $S-1$. In the simplest approach we disentangle [29] spin-orbital superexchange both in the ground and excited state, and use the same frozen AO order as in the initial state to determine spin exchange $J_\diamondsuit$. A spin excitation (a magnon) itself is best described by the transformation to Holstein-Primakoff (HP) bosons. In linear spin-wave theory, the magnon energy consists of two contributions and we introduce:

(i) Ising energy for a localized HP boson $I^{(0)} \equiv 4J_\diamondsuit S$, and

(ii) the propagating term $P^{(0)}(\vec{k}) \equiv -4J_\diamondsuit S\gamma_{\vec{k}}$.

The latter originates from quantum fluctuations $\propto -\frac{1}{2}J_\diamondsuit\big(\hat{S}_i^+\hat{S}_j^- + \hat{S}_i^-\hat{S}_j^+\big)$, where $\gamma_{\vec{k}} = \frac{1}{4}\sum_{\vec{\delta}} e^{i\vec{k}\cdot\vec{\delta}}$ determines the dispersion and depends on the 2D momentum $\vec{k} = (k_a, k_b)$ with $k_\alpha \in [-\pi, \pi)$. Here $\vec{\delta}$ stands for one of four nearest neighbors of the central site $i = 0$ shown in Fig. 11(a). The above two terms determine the magnon dispersion in a 2D ferromagnet,

$$\omega_{\vec{k}}^{(0)} = I^{(0)} + P^{(0)}(\vec{k}) = 4J_\diamondsuit S\,(1-\gamma_{\vec{k}}), \tag{40}$$

which serves as a reference below. The breaking of SU(2) symmetry is reflected by a Goldstone mode (at $\vec{k} = 0$), and $\omega_{\vec{k}} = J_\diamondsuit S k^2$ for $\vec{k} \to 0$ —we find that this result is insensitive to spin-orbital coupling. It is crucial that the above dispersion (40) is improved and the variational approximation (VA) is performed for each value of momentum $\vec{k}$ independently. One might expect that this reduces spin exchange, $J_\diamondsuit \to J_{\blacklozenge}$, and the magnon dispersion would soften. In this way we obtain the renormalized magnon dispersion which replaces Eq. (40),

$$\omega_{\vec{k}}(\{\theta_{iL}\}) = I(\{\theta_{iL}\};\vec{k}) + P(\{\theta_{iL}\};\vec{k}). \tag{41}$$

Note that the angles $\{\theta_{iL}\}$ are real and $L = A, B$ refers to the sublattice. If in addition it is assumed that orbital optimization for both sublattices is equivalent, we use the constraint $\theta_i \equiv \theta_{iA} = \theta_{iB}$ $(i = 1, 2, 3)$ which defines the Simplified Variational Approximation (SVA). Finally, we have verified the predictions of the VA by exact diagonalization employing a Numerical *Ansatz* (NA) with six states per sublattice: a spin defect with or without orbital excitation, and four spin-orbital states with spin excitation at the central site together with an orbital excitation at one of the nearest neighbors. The state with excitations within a shaded cluster depicted in Fig. 11(b) may be thus expressed in terms of these six states.

Taking as an example the K_2CuF_4 state at $E_z = -0.8\,J$ shown in Fig. 11(b), one finds that the orbital renormalization is appreciable—at the central site with spin excitation it is largely modified to $\sim (x^2-y^2)$, and the orbitals at the four neighboring sites are also changed. The latter orbitals found within the VA are only weakly changed as these latter sites have three neighbors belonging to the neighbors with undisturbed AO order in Fig. 11(a), but the one at the site of spin excitation itself is radically different. For this reason, we introduce a cutoff and assume that the orbitals at further neighbors of the excited spin are unchanged. One expects then

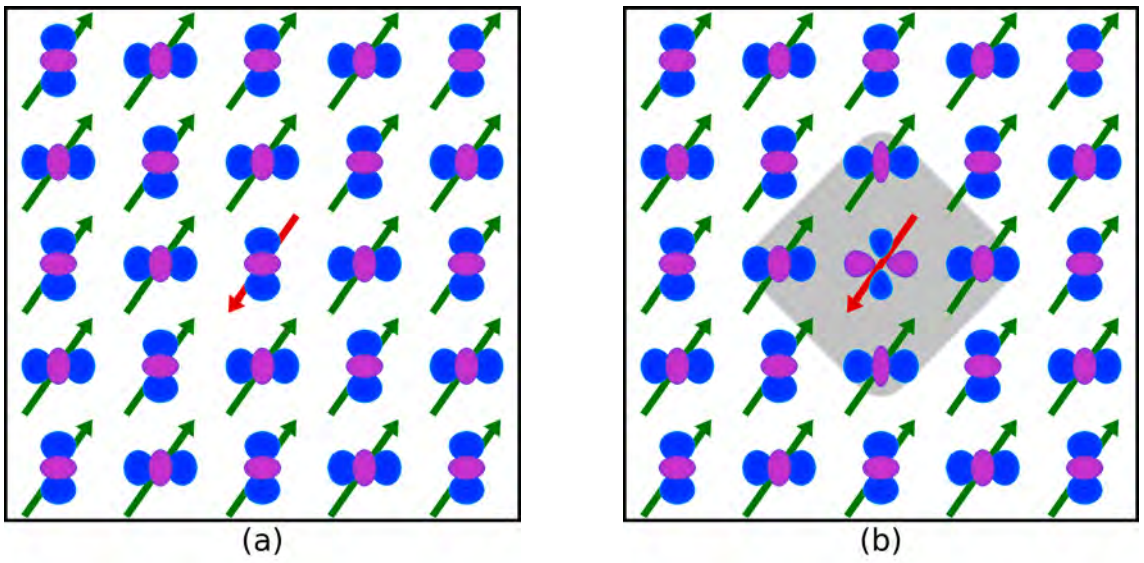

Fig. 11: *Artist's view of a spin excitation (inverted red arrow at the central site) in the FM plane of K_2CuF_4 (green arrows) and AO order of the orbitals occupied by holes at $E_z = -0.8J$, with: (a) frozen orbitals; (b) optimized orbitals at the central site and at four its neighboring sites in the square lattice, forming a quasiparticle (dressed magnon). The above value of E_z leads to the expected AO order in K_2CuF_4, with $\theta_{opt} \simeq 71^\circ$ in Eqs. (14). When the VA is used, case (a) is still realized at $\vec{k} \simeq 0$, while case (b) represents a dressed magnon with $\vec{k} \simeq M$ where orbital states in the shaded cluster are radically different from those shown for frozen orbitals in (a). Image reproduced from Ref. [42].*

a large dressing of the magnon, with the corresponding reduction of the effective FM interaction to $J_{\blacklozenge}$, particularly in the neighborhood of the M point. This is confirmed by the results shown in Fig. 12(a)—the magnon energy ω_M is reduced by $\sim 27\%$ from $\omega_M^{(0)}$. Internal consistency of the theory is confirmed by this reduction being nearly the same in all three methods used to treat spin-orbital coupling: VA, SVA, and NA.

At the X point we recognize the importance of independent optimization of orbitals on the two sublattices—the energy ω_X is reduced by $\sim 25\%$ from $\omega_X^{(0)}$ in the VA, while it stays almost unrenormalized in the SVA, see Fig. 12(a). The NA agrees very well with the results of the VA except for the points close to the M point along the M-Γ path. While the VA may underestimate somewhat the magnon dressing effect, altogether we find a comparison of the VA with the NA very encouraging indeed. The renormalization of the magnon energy increases fast when the orbital splitting $|E_z|$ is reduced, and one finds that the magnon energy reduction is large for $E_z = -0.3\,J$, e.g. by $\sim 60\%$ at the M point, see Fig. 12(b). The agreement between the VA and the NA is somewhat worse here, but still one may say that both methods qualitatively agree. Altogether, we suggest that the magnon softening may be very large for spin-orbital systems with low spin $S = 1/2$ as in K_2CuF_4. Note that similar softening is expected in the FM planes of $LaMnO_3$ and would represent an interesting future research topic.

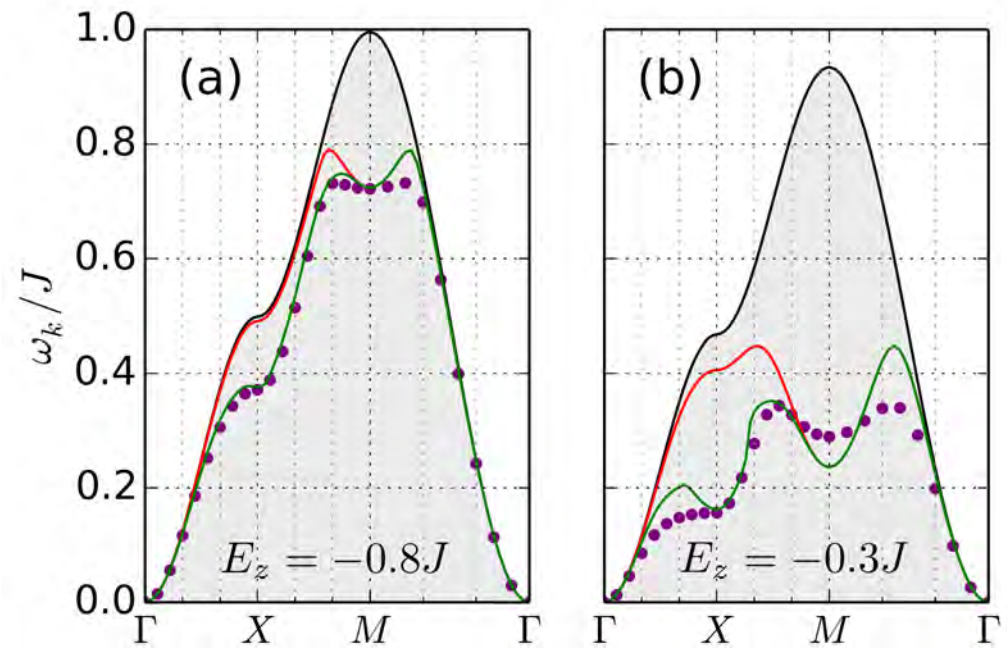

Fig. 12: *The magnon energy $\omega_{\vec{k}}/J$ obtained for the FM state of K_2CuF_4 at $J_H/U = 0.2$ and: (a) $E_z = -0.80J$ and (b) $E_z = -0.30J$. Results are presented for four approximations: frozen orbitals (black line and grey background), the VA (green line), the SVA (red line), and the 12-state NA (purple dots). The high symmetry points are: $\Gamma = (0,0)$, $X = (\pi,0)$, $M = (\pi,\pi)$. Image reproduced from Ref. [42].*

4.3 Weak spin-orbital entanglement for large spins S=2 in $LaMnO_3$

Electronic structure calculations predict A-AF SO, in agreement with experiment [32]. It follows from the spin-orbital superexchange between large spins $S = 2$ in $LaMnO_3$, due to the excitations involving e_g electrons. The energies of the five possible excited states [30] shown in Fig. 6(a) are: (i) the HS ($\mathcal{S} = \frac{5}{2}$) $^6A_1$ state, and (ii) the LS ($\mathcal{S} = \frac{3}{2}$) states: $^4A_1$, ^4E ($^4E_\epsilon$, $^4E_\theta$), and $^4A_2$. They are parameterized again by the intra-orbital Coulomb element U and by Hund's exchange J_H^e between a pair of e_g electrons at a Mn^{2+} (d^5) ion. The Racah parameters $B = 0.107$ eV and $C = 0.477$ eV justify an approximate relation $C \simeq 4B$, and we find the LS excitation spectrum: $\varepsilon(^4A_1) = U + \frac{3}{4}J_H$, $\varepsilon(^4E) = U + \frac{5}{4}J_H$ (twice), and $\varepsilon(^4A_2) = U + \frac{13}{4}J_H$. Using the spin algebra (Clebsch-Gordan coefficients) and considering again two possible e_g orbital configurations on the bonds, see Eqs. (17) and (18), and charge excitations by t_{2g} electrons, one finds a compact expression [43],

$$\mathcal{H}_e = \frac{1}{16}\sum_\gamma \sum_{\langle ij\rangle\parallel\gamma} \Big\{ -\frac{8}{5}\frac{t^2}{\varepsilon(^6A_1)}\Big(\vec{S}_i\cdot\vec{S}_j+6\Big)\mathcal{P}^{(\gamma)}_{\langle ij\rangle} + \Big[\frac{t^2}{\varepsilon(^4E)}+\frac{3}{5}\frac{t^2}{\varepsilon(^4A_1)}\Big]\Big(\vec{S}_i\cdot\vec{S}_j-4\Big)\mathcal{P}^{(\gamma)}_{\langle ij\rangle} + \Big[\frac{t^2}{\varepsilon(^4E)}+\frac{t^2}{\varepsilon(^4A_2)}\Big]\Big(\vec{S}_i\cdot\vec{S}_j-4\Big)\mathcal{Q}^{(\gamma)}_{\langle ij\rangle}\Big\} + E_z\sum_i \tau_i^{(c)}. \quad (42)$$

In addition, t_{2g} electrons also contribute with $\mathcal{H}_t = \frac{1}{8}J\beta r_t\Big(\vec{S}_i\cdot\vec{S}_j-4\Big)$. Here $\beta = (t_\pi/t)^2$ follows from the difference between the effective d-d hopping elements along the σ and π

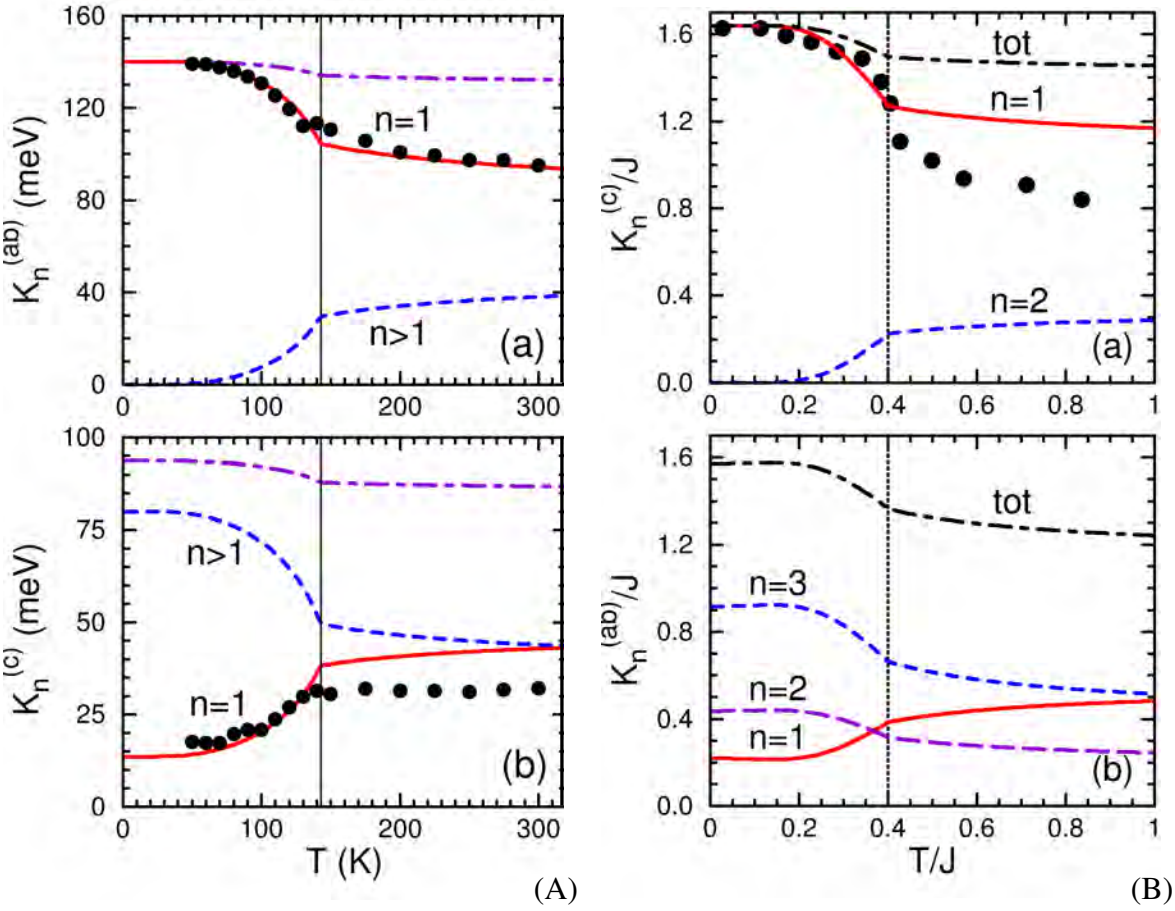

Fig. 13: *Kinetic energies per bond $K_n^{(\gamma)}$ Eq. (32) for increasing temperature T obtained from the respective spin-orbital models for FM (top) and AF (bottom) bonds along the axis γ: (A) LaMnO$_3$ (with $J = 150$ meV, $\eta \simeq 0.18$ [28], and experimental points [33]); (B) LaVO$_3$ with η=0.13 [35] and experimental points [44]. The kinetic energies in HS states ($n = 1$, red lines) are compared with the experiment (filled circles). Vertical dotted lines indicate values of $T_{\rm N}$. Images reproduced from Ref. [28].*

bonds, i.e., $\beta \simeq \frac{1}{9}$, while the coefficient r_t stands for a superposition of all t_{2g} excitations involved in the t_{2g} superexchange [28]. Note that spin-projection operators for high (low) total spin $\mathcal{S} = 2$ ($\mathcal{S} = 1$) cannot be used, but again the HS term stands for a FM contribution which dominates over the LS terms when $\left\langle \mathcal{P}_{\langle ij\rangle}^{(\gamma)} \right\rangle \simeq 1$. Charge excitations by t_{2g} electrons give double occupancies in active t_{2g} orbitals, so $\mathcal{H}_t$ is AF but this term is small—as a result FM interactions may dominate but again only along two spatial directions. Indeed, this happens for the realistic parameters of LaMnO$_3$ for the ab planes where SO is FM and coexists with AO order, while along the c axis SO is AF accompanied by FO order, in agreement with GKR, i.e., spin-orbital order is A-AF/C-AO. Indeed, this type of order is found both from the theory for realistic parameters and from electronic structure calculations [45]. The JT orbital interactions are responsible for the enhanced value of the orbital transition temperature [46].

Spin- and orbital-energy scale separately here, and the OO is mainly triggered by JT distortions [45]. The optical spectral weight due to HS states in LaMnO$_3$ may be easily derived from

the present model (42), following the general theory, see Eq. (32). One finds a very satisfactory agreement between the present theory and the experimental results [33], as shown in Fig. 13(A). We emphasize, that no fit is made here, i.e., the kinetic energies (32) are calculated using the same parameters as those used elsewhere for the magnetic exchange constants [28]. Therefore, such a good agreement with experiment suggests that indeed the spin-orbital superexchange may be disentangled for large $S = 2$ spins. Summarizing, we have found that spin-orbital entanglement is weak in this case [46]. *A posteriori*, this conclusion could be also drawn from a good agreement of spin excitations predicted by the theory with experimental data [47].

5 Spin-orbital entanglement in t_{2g} electron models

5.1 Entangled phases of $LaVO_3$ and YVO_3

In this case one uses the degenerate Hubbard model for three t_{2g} orbitals with J_H^t (22) [48]. Spin-orbital entanglement is stronger for t_{2g} than for e_g systems [29]. Due to large Coulomb interaction, the spin-orbital entangled state in RVO$_3$ ($R =$ La,. . . ,Lu) satisfies in a Mott insulator the local constraint at V^{3+} site i,

$$n_{ia} + n_{ib} + n_{ic} = 2, \tag{43}$$

and G-type OO competes with the spin-orbital entangled state. Rare earth site disorder favors the spin-orbital entanglement rather than a cooperative JT distortion [49]. The entanglement is best seen in the coupling between the spin and orbital phase transition [50]. Due to Hund's exchange J_H, one has here coupled $S = 1$ spins and $\tau = 1/2$ orbitals for three ($n = 1, 2, 3$) charge excitations ε_n arising from the transitions to [see Fig. 6(b)]:

(i) a high-spin state $^4A_2$ at energy $U-3J_H$,
(ii) two degenerate low-spin states $^2T_1$ and ^2E at U, and
(iii) a $^2T_2$ low-spin state at $U+2J_H$ [16].

Using η (25), we parametrize this multiplet structure by r_1, Eq. (36), and the top multiplet state,

$$r_5 = \frac{1}{1+2\eta}. \tag{44}$$

The cubic symmetry is broken and the CF induces orbital splitting in RVO$_3$, hence $\langle n_{ic}\rangle = 1$ and the orbital degrees of freedom are given by the doublet $\{a, b\}$, with $n_{ia} + n_{ib} = 1$, which defines the pseudospin operators $\vec{\tau}_i$ at site i. One derives a HS contribution $H_1^{(c)}(ij)$ for a bond $\langle ij\rangle$ along the c axis, and $H_1^{(ab)}(ij)$ for a bond in the ab plane:

$$H_1^{(c)}(ij) = -\tfrac{1}{3}Jr_1\big(\vec{S}_i\cdot\vec{S}_j + 2\big)\big(\tfrac{1}{4} - \vec{\tau}_i\cdot\vec{\tau}_j\big), \tag{45}$$

$$H_1^{(ab)}(ij) = -\tfrac{1}{6}Jr_1\big(\vec{S}_i\cdot\vec{S}_j + 2\big)\big(\tfrac{1}{4} - \tau_i^z\tau_j^z\big). \tag{46}$$

In Eq. (45) pseudospin operators $\vec{\tau}_i$ describe the low-energy dynamics of (initially degenerate) $\{xz, yz\}$ orbital doublet at site i; this dynamics is quenched in the plane, see $H_1^{(ab)}$ Eq. (46).

Here $\frac{1}{3}(\vec{S}_i\cdot\vec{S}_j+2)$ is the projection operator on the HS state for $S=1$ spins. The terms $H_n^{(c)}(ij)$ for LS excitations ($n=2,3$) contain instead the spin operator $(1-\vec{S}_i\cdot\vec{S}_j)$ (which guarantees that these terms cannot contribute for fully polarized spins $\langle\vec{S}_i\cdot\vec{S}_j\rangle=1$):

$$\begin{aligned} H_2^{(c)}(ij) &= -\tfrac{1}{12}\,J\,\big(1-\vec{S}_i\cdot\vec{S}_j\big)\big(\tfrac{7}{4}-\tau_i^z\tau_j^z-\tau_i^x\tau_j^x+5\tau_i^y\tau_j^y\big),\\ H_3^{(c)}(ij) &= -\tfrac{1}{4}Jr_5\big(1-\vec{S}_i\cdot\vec{S}_j\big)\big(\tfrac{1}{4}+\tau_i^z\tau_j^z+\tau_i^x\tau_j^x-\tau_i^y\tau_j^y\big). \end{aligned} \tag{47}$$

Again the terms $H_n^{(ab)}(ij)$ differ from $H_n^{(c)}(ij)$ only by the orbital operators,

$$\begin{aligned} H_2^{(ab)}(ij) &= -\tfrac{1}{8}\,J\,\big(1-\vec{S}_i\cdot\vec{S}_j\big)\big(\tfrac{19}{12}\mp\tfrac{1}{2}\tau_i^z\mp\tfrac{1}{2}\tau_j^z-\tfrac{1}{3}\tau_i^z\tau_j^z\big),\\ H_3^{(ab)}(ij) &= -\tfrac{1}{8}Jr_5\big(1-\vec{S}_i\cdot\vec{S}_j\big)\big(\tfrac{5}{4}\mp\tfrac{1}{2}\tau_i^z\mp\tfrac{1}{2}\tau_j^z+\tau_i^z\tau_j^z\big), \end{aligned} \tag{48}$$

where upper (lower) sign corresponds to bonds along the a (b) axis.
First, we present a mean field approximation for the spin and orbital bond correlations which are determined self-consistently after decoupling them from each other in $\mathcal{H}_J$ (28). Spin interactions in Eq. (29) are given by two exchange constants:

$$\begin{aligned} J_c &= \tfrac{1}{2}J\left\{\eta r_1-(r_1-\eta r_1-\eta r_5)(\tfrac{1}{4}+\langle\vec{\tau}_i\cdot\vec{\tau}_j\rangle)-2\eta r_5\langle\tau_i^y\tau_j^y\rangle\right\},\\ J_{ab} &= \tfrac{1}{4}J\left\{1-\eta r_1-\eta r_5+(r_1-\eta r_1-\eta r_5)(\tfrac{1}{4}+\langle\tau_i^z\tau_j^z\rangle)\right\}, \end{aligned} \tag{49}$$

determined by orbital correlations $\langle\vec{\tau}_i\cdot\vec{\tau}_j\rangle$ and $\langle\tau_i^\alpha\tau_j^\alpha\rangle$. By evaluating them one finds $J_c<0$ and $J_{ab}>0$ and the C-AF SO is supported.
In the orbital sector one finds at the same time,

$$H_\tau = \sum_{\langle ij\rangle_c}\left[J_c^\tau\vec{\tau}_i\cdot\vec{\tau}_j-J(1-s_c)\eta r_5\tau_i^y\tau_j^y\right]+J_{ab}^\tau\sum_{\langle ij\rangle_{ab}}\tau_i^z\tau_j^z, \tag{50}$$

$$J_c^\tau = \tfrac{1}{2}J\left[(1+s_c\,)r_1+(1-s_c\,)\eta(r_1{+}r_5)\right], \tag{51}$$

$$J_{ab}^\tau = \tfrac{1}{4}J\left[(1-s_{ab})r_1+(1+s_{ab})\eta(r_1{+}r_5)\right], \tag{52}$$

depending on spin correlations: $s_c=\langle\vec{S}_i\cdot\vec{S}_j\rangle_c$ and $s_{ab}=-\langle\vec{S}_i\cdot\vec{S}_j\rangle_{ab}$. In a classical C-AF state ($s_c=s_{ab}=1$) this mean field procedure becomes exact, and the orbital problem maps to Heisenberg pseudospin chains along the c axis, weakly coupled (as $\eta\ll1$) along a and b bonds,

$$H_\tau^{(0)}=Jr_1\left[\sum_{\langle ij\rangle_c}\vec{\tau}_i\cdot\vec{\tau}_j+\frac{1}{2}\eta\left(1+\frac{r_5}{r_1}\right)\sum_{\langle ij\rangle_{ab}}\tau_i^z\tau_j^z\right], \tag{53}$$

releasing large zero-point energy. Thus, spin C-AF and G-AO order with quasi-1D orbital quantum fluctuations support each other in RVO$_3$. Orbital fluctuations play here a prominent role and amplify the FM exchange J_c, making it even stronger than the AF exchange J_{ab} [16].
Having the individual terms $H_n^{(\gamma)}$ of the spin-orbital model, one may derive the spectral weights of optical spectra, see Eq. (32). The HS excitations have remarkable temperature dependence and the spectral weight decreases in the vicinity of the magnetic transition at $T_{\rm N}$, see Fig. 13(B). The observed behavior is reproduced in the theory only when spin-orbital interactions are treated in a cluster approach, i.e., they *cannot* be disentangled.

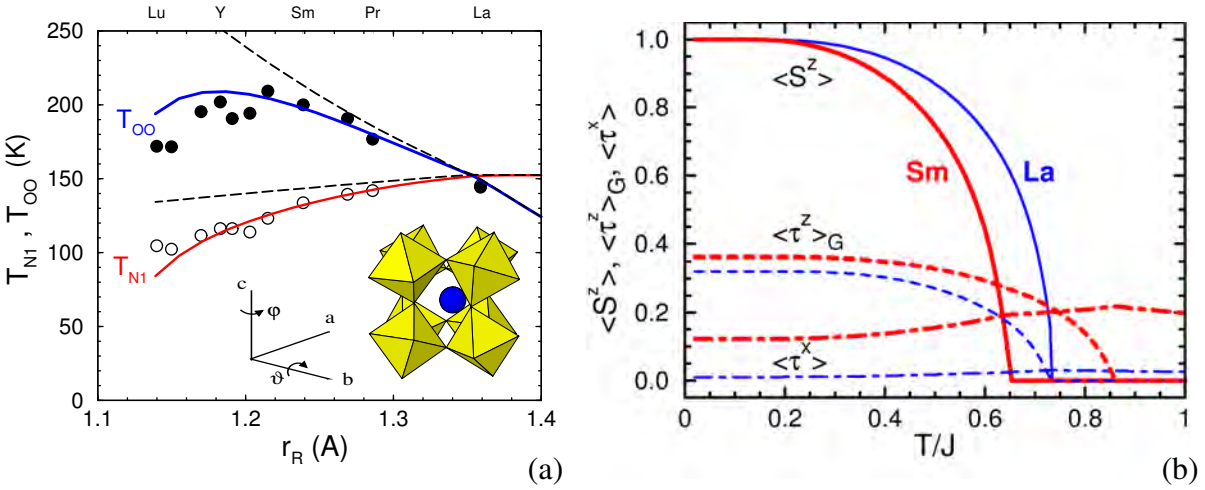

Fig. 14: *Phase transitions in the vanadium perovskites RVO_3: (a) phase diagram with the orbital $T_{\rm OO}$ and Néel $T_{\rm N1}$ transition temperatures obtained from the theory with and without orbital-lattice coupling (solid and dashed lines) [50], and from experiment (circles) [51]; (b) spin $\langle S_i^z\rangle$ (solid) and G-type orbital $\langle\tau_i^z\rangle_G$ (dashed) order parameters, vanishing at $T_{\rm N1}$ and $T_{\rm OO}$, respectively, and the transverse orbital polarization $\langle\tau_i^x\rangle$ (dashed-dotted lines) for $LaVO_3$ and $SmVO_3$ (thin and heavy lines). Images reproduced from Ref. [50].*

Unlike in $LaMnO_3$ where the spin and orbital phase transitions are well separated [46], in the RVO_3 ($R =$ Lu, Yb,. . . ,La) the two above transitions are close to each other [51]. It is not easy to reproduce the observed dependence of the transition temperatures $T_{\rm OO}$ and the Néel T_{N1} on the ionic radius r_R (in the RVO_3 compounds with small r_R there is also another magnetic transition at T_{N2} [52] which is not discussed here). The spin-orbital model was extended by the coupling to the lattice to unravel a nontrivial interplay between superexchange, the orbital-lattice coupling due to the $GdFeO_3$-like rotations of the VO_6 octahedra, and orthorhombic lattice distortions [50]. One finds that the lattice strain affects the onset of the magnetic and orbital order by partial suppression of orbital fluctuations, and the dependence of $T_{\rm OO}$ is non-monotonous, while T_{N1} is reduced, see Fig. 14(a). Thereby the orbital polarization $\propto \langle\tau^x\rangle$ increases with decreasing ionic radius r_R, see Fig. 14(b). The theoretical approach [50] demonstrates that orbital-lattice coupling is very important and reduces both $T_{\rm OO}$ and Néel T_{N1} for small ionic radii. Simultaneously, T_{N1} decreases to the left due to spin-orbital entanglement.

It has also been shown that the t_{2g} perovskite $LaVO_3$ is a unique case where the KK phase transition drives orbital order, in contrast to the usual case where the OO is controlled by the CF splitting enhanced by Coulomb interaction and both OO and SO transition are well separated [53]. As a consequence, the magnetic transition is close to (and even above) the superexchange driven OO order transition, and $T_{\rm N} > T_{\rm KK} \sim T_{OO}$, whereas typically magnetism arises at much lower temperatures than orbital ordering. In contrast, in YVO_3 the CF is sufficiently large to suppress the KK phase transition and spin-orbital interactions disentangle.

5.2 Spin-orbital entanglement on a triangular lattice

Finally, we wish to discuss here two rather interesting examples going also beyond the perovskite lattice, involving d^1 configurations. Two operators are entangled if their states at temperature $T = 0$ cannot be factorized into parts belonging to different subspaces. This happens precisely in some spin-orbital models and is the source of spin-orbital entanglement [29]. To verify whether entanglement occurs or not, it suffices to compute and analyze the spin, orbital and spin-orbital (four-operator) correlation functions for a bond $\langle ij\rangle$ along γ axis, given by

$$\begin{aligned}
S_{ij} &\equiv \tfrac{1}{d}\,\textstyle\sum_n \big\langle n\big|\vec{S}_i\cdot\vec{S}_j\big|n\big\rangle\,, &(54)\\
T_{ij} &\equiv \tfrac{1}{d}\,\textstyle\sum_n \big\langle n\big|(\vec{T}_i\cdot\vec{T}_j)^{(\gamma)}\big|n\big\rangle\,, &(55)\\
C_{ij} &\equiv \tfrac{1}{d}\,\textstyle\sum_n \big\langle n\big|(\vec{S}_i\cdot\vec{S}_j - S_{ij})\,(\vec{T}_i\cdot\vec{T}_j - T_{ij})^{(\gamma)}\big|n\big\rangle &(56)\\
&= \tfrac{1}{d}\,\textstyle\sum_n \big\langle n\big|(\vec{S}_i\cdot\vec{S}_j)(\vec{T}_i\cdot\vec{T}_j)^{(\gamma)}\big|n\big\rangle - \Big(\tfrac{1}{d}\textstyle\sum_n \big\langle n\big|\vec{S}_i\cdot\vec{S}_j\big|n\big\rangle\Big)\Big(\tfrac{1}{d}\textstyle\sum_m \big\langle m\big|(\vec{T}_i\cdot\vec{T}_j)^{(\gamma)}\big|m\big\rangle\Big),
\end{aligned}$$

where d is the ground state degeneracy, and the pseudospin scalar product in Eqs. (55) and (56) is relevant for a model with active t_{2g} orbital degrees of freedom. As a representative example we evaluate here such correlations for a 2D spin-orbital model derived for a $NaTiO_2$ plane [54]; other situations with spin-orbital entanglement are discussed in Ref. [29].

To explain the physical origin of the spin-orbital model for $NaTiO_2$ [54], we consider a representative bond along the c axis shown in Fig. 15. For the realistic parameters of $NaTiO_2$ the t_{2g} electrons are almost localized in d^1 configurations of Ti^{3+} ions, hence their interactions with neighboring sites can be described by the effective superexchange and kinetic exchange processes. Virtual charge excitations between the neighboring sites, $d_i^1 d_j^1 \rightleftharpoons d_i^2 d_j^0$, generate magnetic interactions which arise from two different hopping processes for active t_{2g} orbitals: (i) the effective hopping $t = t_{pd}^2/\Delta$ which occurs via oxygen $2p_z$ orbitals with the charge transfer excitation energy Δ, in the present case along the 90° bonds, and (ii) direct hopping t' which couples the t_{2g} orbitals along the bond and gives a kinetic exchange interaction, as in the Hubbard model (2). Note that the latter processes couple orbitals with the same flavor, while the former ones couple different orbitals (for this geometry) so the occupied orbitals may be interchanged as a result of a virtual charge excitation—these processes are shown in Fig. 15.

The effective spin-orbital model considered here for $NaTiO_2$ reads [54],

$$\mathcal{H} = J\left((1-\alpha)\,\mathcal{H}_s + \sqrt{(1-\alpha)\alpha}\,\mathcal{H}_m + \alpha\,\mathcal{H}_d\right). \tag{57}$$

The parameter α in Eq. (57) is given by the hopping elements as follows,

$$\alpha = (t')^2/\left[t^2 + (t')^2\right]\,, \tag{58}$$

and interpolates between the superexchange $\mathcal{H}_s$ ($\alpha = 0$) and kinetic exchange $\mathcal{H}_d$ ($\alpha = 1$), while in between these two exchange elements and mixed exchange $\mathcal{H}_m$ contributes simultaneously; these terms are explained in Ref. [54]. This model is considered here in the absence of Hund's exchange η (25), i.e., at $\eta = 0$. One finds that all the orbitals contribute equally in the entire range of α, and each orbital state is occupied at two out of six sites in the entire regime of

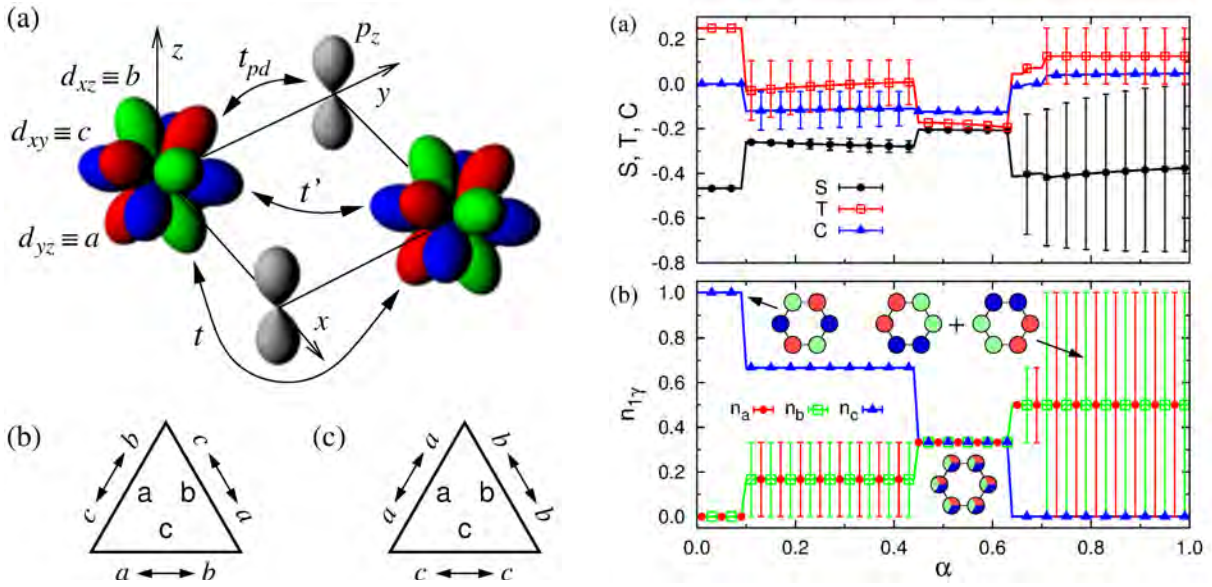

Fig. 15: *Left — (a) Hopping processes between t_{2g} orbitals along a bond parallel to the c axis in $NaTiO_2$: (i) t_{pd} between Ti(t_{2g}) and O($2p_z$) orbitals—two t_{pd} transitions define an effective hopping t, and (ii) direct d-d hopping t'. The t_{2g} orbitals (7) are shown by different color. The bottom part gives the hopping processes along the $\gamma = a, b, c$ axes that contribute to Eq. (57): (b) superexchange and (c) direct exchange. Right — Ground state for a free hexagon as a function of α: (a) bond correlations—spin S_{ij} Eq. (54) (circles), orbital T_{ij} Eq. (55) (squares), and spin–orbital C_{ij} Eq. (56) (triangles); (b) orbital electron densities $n_{1\gamma}$ at a representative site $i = 1$ (left-most site): n_{1a} (circles), n_{1b} (squares), n_{1c} (triangles). The insets indicate the orbital configurations favored by the superexchange $(\alpha = 0)$, by mixed interactions $0.44 < \alpha < 0.63$, and by the direct exchange $(\alpha = 1)$. The vertical lines indicate an exact range of configurations due to the degeneracy. Images reproduced from Ref. [55].*

α, see Fig. 15. The orbital state changes under increasing α and one finds as a result four distinct regimes, with abrupt transitions between them. In the superexchange model ($\alpha = 0$) there is precisely one orbital at each site which contributes, e.g. $n_{1c} = 1$ as the c orbital is active along both bonds. Having a frozen orbital configuration, the orbitals decouple from spins and the ground state is disentangled, with $C_{ij} = 0$, and one finds that the spin correlations $S_{ij} = -0.4671$, as for the AF Heisenberg ring of $L = 6$ sites. Orbital fluctuations increase gradually with increasing α and this results in finite spin-orbital entanglement $C_{ij} \simeq -0.12$ for $0.10 < \alpha < 0.44$; simultaneously spin correlations weaken to $S_{ij} \simeq -0.27$.

In agreement with intuition, when $\alpha = 0.5$ and all inter-orbital transitions shown in Fig. 15 have equal amplitude, there is large orbital mixing which is the most prominent feature in the intermediate regime of $0.44 < \alpha < 0.63$. Although spins are coupled by AF exchange, the orbitals fluctuate here strongly and reduce further spin correlations to $S_{ij} \simeq -0.21$. The orbital correlations are negative, $T_{ij} < 0$, the spin-orbital entanglement is finite, $C_{ij} \simeq -0.13$, and the ground state is unique ($d = 1$). Here all the orbitals contribute equally and $n_{1\gamma} = 1/3$ which may be seen as a precursor of the spin-orbital liquid state which dominates the behavior of the triangular lattice. The regime of larger values of $\alpha > 0.63$ is dominated by the kinetic exchange

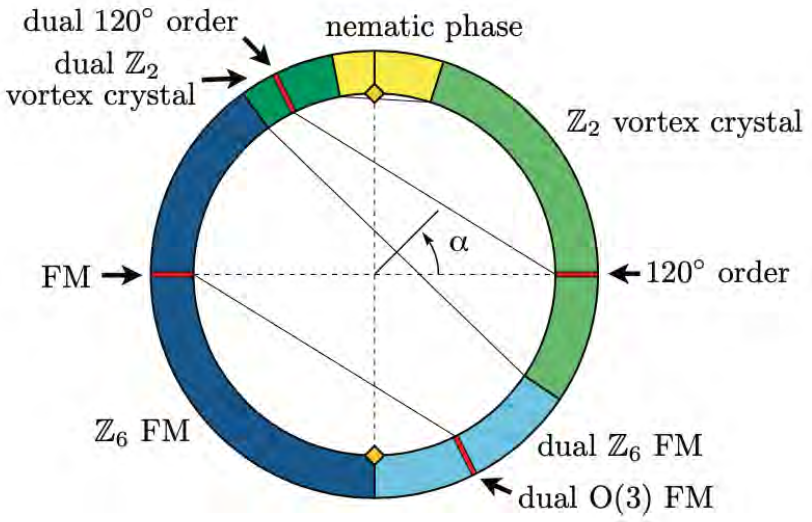

Fig. 16: *Phase diagram of the Kitaev-Heisenberg model Eq.* (59) *with parametrization* $(J, K) = (\cos\alpha, \sin\alpha)$ *as obtained from exact diagonalization data. Solid lines show the mapping between two Klein-dual points. Red lines mark the location of the four SU(2)—symmetric points. Yellow diamonds mark the two Kitaev points. Image reproduced from Ref. [56].*

in Eq. (57), and the ground state is degenerate with $d = 2$ [55], with strong scattering of possible electron densities $\{b_{i\gamma}\}$, see Fig. 15. Weak entanglement is found for $\alpha > 0.63$, where $C_{ij} \simeq 0$. Summarizing, except for the regimes of $\alpha < 0.09$ and $\alpha > 0.63$, the ground state of a single hexagon is strongly entangled, i.e., $C_{ij} < -0.10$, see Fig. 15.

As the last example we would like to highlight briefly the Heisenberg-Kitaev (HK) Hamiltonian on the triangular lattice [56]. Here spin-orbital entanglement is triggered by formation of effective $j = 1/2$ spins in a Mott insulator observed for the recently synthesized $Ba_2IrTi_2O_9$. The model is frustrated, both by its interactions and by geometry, see Fig. 16. The description of the microscopic physics is given here by a superposition of Heisenberg and Kitaev interaction,

$$\mathcal{H}_{HK} = J \sum_{\langle ij \rangle} \left(\vec{S}_i \cdot \vec{S}_j \right) + K \sum_{\gamma \| \langle ij \rangle} S_i^\gamma \, S_j^\gamma, \tag{59}$$

where $\vec{S}_i$ is a spin operator located on site i of the triangular lattice spanned by the lattice vectors $\vec{a}_x = (1, 0)^T$, $\vec{a}_y = (-1/2, \sqrt{3}/2)^T$, and $\vec{a}_z = -\vec{a}_x - \vec{a}_y$, for the lattice constant $a = 1$. The first term is the Heisenberg coupling $\propto J$, while the Kitaev term $\propto K$ explicitly breaks spin-rotation invariance and acts only between the same spin components $S_i^\gamma S_j^\gamma$ at nearest neighbor sites.

First, we observe that an infinitesimal Kitaev exchange removes the $120°$ order of the quantum Heisenberg model [56]. Second, the phase diagram of Fig. 16 is very rich and instead of $120°$ order, an extended $\mathbb{Z}_2$-vortex crystal phase arises which could be identified experimentally. Third, the phase diagram exhibits a duality, similar to the HK model on the honeycomb lattice [57]. This duality relates a pair of interactions on the right-hand side of the circle to a pair of interactions on the left-hand side, i.e., $J \to -J$ and $K \to 2J+K$. The corresponding dual states are related by a four-sublattice basis transformation. For more explanation see Ref. [56].

6 Experimental consequences of spin-orbital entanglement

The field of spin-orbital physics is recently growing and becoming richer due to new experiments. Understanding them is possible within simple models, mainly developed in low dimension. Also there entanglement is the strongest as quantum phenomena domininate in low dimension. We shall concentrate on them here as they uncover important principles of treating spin-orbital entanglement, both in the ground and in excited states. Spin-orbital entangled states occur in several quantum materials and the proper understanding of them becomes crucial for the quantitative analysis of the observed thermodynamic phase transitions.

Let us summarize briefly entanglement properties which could modify the experiment. First, I would like to recall the 1D chain, where each of the fractional quasiparticles carries both spin and orbital quantum numbers, and the two variables (spin and orbital) are always entangled in the collective excitations [58]. The spin-orbital chain with two orbital flavors has been carefully studied, both without the orbital spitting [e.g. in the SU(4) case] and for large splitting E_z.

Second, the 1D cuprate $CaCu_2O_3$ is a good example for the spin-orbital fractionalization along the chain direction, while at the same time no fractionalization is observed for the xy orbital which extends in both leg and rung direction [59]. Thus different degrees of dimensionality may be selected by orbitals and thus the entanglement depends on particular orbitals involved in the hopping. In a realistic 1D model for $CaCu_2O_3$ the splitting between the LS and HS terms occurs for finite Hund's exchange J_H. In fact, any spin-orbital model requires to include a finite, but realistic Hund's exchange to explain the experimental data [60].

Third, another important competitor to the spin-orbital physics and on-bond entanglement is the strong JT effect which is found as well in $KCuF_3$ [61]. It drives the orbital order and does change d-d excitations which become highly localized. At the same time, the low-energy excitations present clear dispersion. They match extremely well with the two-spinon continuum. So, we suggest that spin-orbital entanglement is a subtle property which is easily destroyed by some stronger local interaction, and the entanglement depends then strongly on the possible coupling to the lattice.

Fourth, spin-orbital coupling may lead to the disappearance of magnetic properties if it is sufficiently strong, removes the orbital degrees of freedom, and generates local singlets [62]. It is then challenging to study exchange interactions between these local singlets. In perovskites one finds a conventional Bose condensation of excitons into a magnetic state, while an unexpected 1D behavior supporting spin-liquid states emerges in honeycomb lattices. When spin and orbital channels are decoupled and orbital frustration induces then frustration in the spin channel, opening up the possibility of spin-orbital liquids with both spin and orbital entanglement [63].

Finally, the physics will change completely when spin-orbit interaction dominates over the superexchange. Then local singlets form and are only weakly coupled by inter-site terms [64]. As we have shown on the example of a 1D spin-orbital chain, entanglement is then strong but preferably limited to a single site, while the inter-site spin-orbital entanglement (which involves superexchange bonds) might be still induced as shown in Sec. 1.

7 Summary

Here we have focused on the interplay of spin and orbital degrees of freedom in realistic Mott insulators and have shown that even when the entanglement is absent, these two types of degrees of freedom (spin and orbital) decide about rather complex behavior, with competing tendencies to localize due to strong correlations and to delocalize to gain more kinetic energy. Quantum fluctuations are particularly well developed in the t_{2g} systems where they partly even destroy OO. As a result, a second order phase transition from the spin-orbital entangled state to a C-OO/G-AF ground state is induced in $LaVO_3$, where the long-range OO suppresses the spin-orbital entanglement [49]. On the other hand, entanglement may be easily removed by phase transitions, as a more fragile property of Mott insulators. It is near a phase transition that spin-orbital entanglement is quenched locally [41]. The detailed energy balance depends as well on the distribution of charge defects which also destroy spin-orbital entanglement locally.
Spin-orbital entanglement in the excited states is almost unexplored and awaits careful future studies. It may be responsible for the modified dispersion of spin (and orbital) excitations when either the spin or the orbital background is modified [42]. Yet, such modifications do not require that the local degrees of freedom factorize, but it suffices that their coupling is modified and causes measurable yet still unexplored properties.
Summarizing, spin-orbital entanglement is an important yet subtle property of Mott insulators. It is fragile and helps to understand how spins and orbitals complement each other and behave in the opposite way in ordered 3D materials. Perhaps the best example is the orbital liquid where orbital disorder coexists with FM order of spins in the ground state of CMR manganites. Then the spin-orbital entanglement is removed and the coherent spin FM order decouples from the orbitals [21]. Many properties of correlated insulators are still unexplored and hopefully will be investigated in the future. This concerns in particular the spin and orbital excitations. We should be prepared that this field has still some hidden surprises to discover and that some of them will be revealed gradually in the future.

Acknowledgments

I thank Wojciech Brzezicki, Louis Felix Feiner, Peter Horsch, Giniyat Khaliullin, Krzysztof Wohlfeld, Jan Zaanen, and Karol Życzkowski for numerous useful discussions and comments. I acknowledge National Science Centre (NCN, Poland) Project No. 2021/43/B/ST3/02166.

References

[1] K.I. Kugel and D.I. Khomskii, Sov. Phys. Usp. **25**, 231 (1982)

[2] P.W. Anderson, Phys. Rev. **115**, 2 (1959)

[3] D.I. Khomskii, *Transition Metal Compounds* (Cambridge University Press, Cambridge, 2014)

[4] Y. Yamashita, N. Shibata, and K. Ueda, Phys. Rev. B **58**, 9114 (1998)

[5] B. Frischmuth, F. Mila, and M. Troyer, Phys. Rev. Lett. **82**, 835 (1999)

[6] Y. Chen, Z.W. Wang, Y.Q. Li, and F.C. Zhang, Phys. Rev. B **75**, 195113 (2007)

[7] A.M. Oleś, Phys. Rev. B **28**, 327 (1983)

[8] K.A. Chao, J. Spałek, and A.M. Oleś, J. Phys. C **10**, L271 (1977)

[9] L.F. Feiner, A.M. Oleś, and J. Zaanen, Phys. Rev. Lett. **78**, 2799 (1997)

[10] L.F. Feiner, A.M. Oleś, and J. Zaanen, J. Phys.: Condens. Matter **10**, L555 (1998)

[11] A.M. Oleś, G. Khaliullin, P. Horsch, and L.F. Feiner, Phys. Rev. Lett. **96**, 147205 (2006)

[12] G. Khaliullin, Prog. Theor. Phys. Suppl. **160**, 155 (2005)

[13] A. Kitaev and J. Preskill, Phys. Rev. Lett. **96**, 110404 (2006)

[14] W. Witczak-Krempa, G. Chen, Y.B. Kim, and L. Balents, Annu. Rev. Condens. Matter Phys. **5**, 57 (2014)

[15] D. Gotfryd, E.M. Pärschke, J. Chaloupka, A.M. Oleś, and K. Wohlfeld, Phys. Rev. Research **2**, 013353 (2020)

[16] G. Khaliullin, P. Horsch, and A.M. Oleś, Phys. Rev. Lett. **86**, 3879 (2001)

[17] P. Horsch, G. Khaliullin, and A.M. Oleś, Phys. Rev. Lett. **91**, 257203 (2003)

[18] G. Jackeli and G. Khaliullin, Phys. Rev. Lett. **103**, 067205 (2009)

[19] N. Goldman and J. Dalibard, Phys. Rev. X **4**, 031027 (2014)

[20] C. Slater and G.F. Koster, Phys. Rev. **94**, 1498 (1954)

[21] L.F. Feiner and A.M. Oleś, Phys. Rev. B **71**, 144422 (2005)

[22] J. van den Brink, P. Horsch, F. Mack, and A.M. Oleś, Phys. Rev. B **59**, 6795 (1999)

[23] L.F. Feiner and A.M. Oleś, Phys. Rev. Research **4**, 043134 (2022)

[24] W. Metzner and D. Vollhardt, Phys. Rev. Lett. **62**, 324 (1989)

[25] M.C. Gutzwiller, Phys. Rev. Lett. **10**, 159 (1963)

[26] W. Metzner, Z. Phys. B **77**, 253 (1989)

[27] Y. Nagaoka, Phys. Rev. **147**, 392 (1966)

[28] A.M. Oleś, G. Khaliullin, P. Horsch, and L.F. Feiner, Phys. Rev. B **72**, 214431 (2005)

[29] A.M. Oleś, J. Phys.: Condens. Matter **24**, 313201 (2012)

[30] J.S. Griffith, *The Theory of Transition Metal Ions* (Cambridge University Press, Cambridge, 1971)

[31] E. Dagotto, T. Hotta, and A. Moreo, Physics Reports **344**, 1 (2001)

[32] Q. Huang, A. Santoro, J.W.Lynn, R.W. Erwin, J.A. Borchers, J.L. Peng, and R.L. Greene, Phys. Rev. B **55**, 14997 (1997)

[33] N.N. Kovaleva, A.M. Oleś, A.M. Balbashov, A. Maljuk, D.N. Argyriou, G. Khaliullin, and B. Keimer, Phys. Rev. B **81**, 235130 (2010)

[34] P. Czarnik, J. Dziarmaga, and A.M. Oleś, Phys. Rev. B **86**, 014420 (2017)

[35] G. Khaliullin, P. Horsch, and A.M. Oleś, Phys. Rev. B **70**, 195103 (2004)

[36] J.B. Goodenough, *Magnetism and the Chemical Bond* (Interscience, New York, 1963)

[37] W. Brzezicki, J. Phys.: Condens. Matter **32**, 313201 (2020)

[38] K. Wohlfeld, M. Daghofer, and A.M. Oleś, EPL—Europhys. Lett. **96**, 27001 (2011)

[39] K. Wohlfeld, M. Daghofer, S. Nishimoto, G. Khaliullin, and J. van den Brink, Phys. Rev. Lett. **107**, 147201 (2011)

[40] A.M. Oleś, L.F. Feiner, and J. Zaanen, Phys. Rev. B **61**, 6257 (2000)

[41] W. Brzezicki, J. Dziarmaga, and A.M. Oleś, Phys. Rev. Lett. **109**, 237201 (2012)

[42] M. Snamina and A.M. Oleś, New J. Phys. **21**, 023018 (2019)

[43] L.F. Feiner and A.M. Oleś, Phys. Rev. B **59**, 3295 (1999)

[44] S. Miyasaka, Y. Okimoto, and Y. Tokura, J. Phys. Soc. Jpn. **71**, 2086 (2002)

[45] E. Pavarini and E. Koch, Phys. Rev. Lett. **104**, 086402 (2010)

[46] M. Snamina and A.M. Oleś, Phys. Rev. B **94**, 214426 (2016)

[47] A.M. Oleś and L.F. Feiner, Phys. Rev. B **65**, 052414 (2002)

[48] N. Chikano, S. Hoshino, and H. Shinaoka, Phys. Rev. B **104**, 235125 (2021)

[49] J.-Q. Yan, W. Tian, H.B. Cao, S. Chi, F. Ye, A. Llobet, A. Puretzky, Q. Chen, J. Ma, Y. Ren, J.-G. Cheng, J.-S. Zhou, M.A. McGuire, and R.J. McQueeney, Phys. Rev. B **100**, 184423 (2019)

[50] P. Horsch, A.M. Oleś, L.F. Feiner, and G. Khaliullin, Phys. Rev. Lett. **100**, 167205 (2008)

[51] S. Miyasaka, Y. Okimoto, M. Iwama, and Y. Tokura, Phys. Rev. B **68**, 100406(R) (2002)

[52] J. Fujioka, T. Yasue, S. Miyasaka, Y. Yamasaki, T. Arima, H. Sagayama, T. Inami, K. Ishii, and Y. Tokura, Phys. Rev. B **82**, 144425 (2010)

[53] X.-J. Zhang, E. Koch, and E. Pavarini, Phys. Rev. B **106**, 115110 (2022)

[54] B. Normand and A.M. Oleś, Phys. Rev. B **78**, 094427 (2008)

[55] J. Chaloupka and A.M. Oleś, Phys. Rev. B **83**, 094406 (2011)

[56] M. Becker, M. Herrmanns, B. Bauer, M. Garst, and S. Trebst, Phys. Rev. B **91**, 155135 (2015)

[57] J. Chaloupka, G. Jackeli, and G. Khaliullin, Phys. Rev. Lett. **110**, 097204 (2013)

[58] C.-C. Chen, M. van Veenendaal, T.P. Devereaux, and K. Wohlfeld, Phys. Rev. B **91**, 165102 (2015)

[59] V. Bisogni, K. Wohlfeld, S. Nishimoto, C. Monney, J. Trinckauf, K. Zhou, R. Klaus, K. Koepernik, C. Sekar, V. Strocov, B. Büchner, T. Schmitt, J. van den Brink, and J. Geck, Phys. Rev. Lett. **114**, 096402 (2015)

[60] R. Fumagalli, J. Heverhagen, D. Betto, R. Arpaia, M. Rossi, D. Di Castro, N.B. Brookes, M. Moretti Sala, M. Daghofer, L. Braicovich, K. Wohlfeld, and G. Ghiringhelli, Phys. Rev. B **101**, 205117 (2020)

[61] J. Li, L. Xu, M. Garcia-Fernandez, A. Nag, H.C. Robarts, A.C. Walters, X. Liu, J. Zhou, K. Wohlfeld, J. van den Brink, H. Ding, and K.-J. Zhou, Phys. Rev. Lett. **126**, 106401 (2021)

[62] G. Khaliullin, Phys. Rev. Lett. **111**, 197201 (2013)

[63] C. Svoboda, M. Randeria, and N. Trivedi, Phys. Rev. B **95**, 014409 (2017)

[64] E.M. Plotnikova, M. Daghofer, J. van den Brink, and K. Wohlfeld, Phys. Rev. Lett. **116**, 106401 (2016)